6-9-2016

ANALYSIS OF BRAZILIAN SPLIT CYLINDER USING THE STATE BASED PERIDYNAMIC LATTICE MODEL

Shreya Vemuganti

Shreya Vemuganti

Candidate

Civil Engineering

Department

This thesis is approved, and it is acceptable in quality and form for publication:

Approved by the Thesis Committee:

Dr. Walter Gerstle , Chairperson

Dr. Mahomoud Reda Taha

Dr. Yu-Lin Shen

ANALYSIS OF BRAZILIAN SPLIT CYLINDER USING THE STATE BASED PERIDYNAMIC LATTICE MODEL

By

SHREYA VEMUGANTI

B.E., CIVIL ENGINEERING, OSMANIA UNIVERSITY, INDIA, 2014

M.S., CIVIL ENGINEERING, UNIVERSITY OF NEW MEXICO, USA, 2016

THESIS

Submitted in Partial Fulfillment of the
Requirement for the Degree of

Master of Science
Civil Engineering

The University of New Mexico
Albuquerque, New Mexico

May, 2016

DEDICATION

To my advisor and mentor Dr. Walter Gerstle

My parents

Seetha and Sreekanth Vemuganti

My sister and brother-in-law

Shloka and Sarat Kompalli

My nephews

Swaraj and Shivaansh Kompalli

I love you!

ACKNOWLEDGEMENTS

I am extremely thankful to my advisor and mentor, Dr. Walter Gerstle for giving me the opportunity to learn and evolve. This research is possible because of his support.

I thank my family for their endless support and undoubted confidence in me. I sincerely thank my committee, Dr. Mahmoud Reda Taha and Dr. Yu Lin Shen. I thank the Civil Engineering Department, University of New Mexico.

Words are powerless to thank RahulReddy ChennaReddy and Moneeb Genedy for their unfailing encouragement.

ANALYSIS OF BRAZILIAN SPLIT CYLINDER USING THE STATE BASED PERIDYNAMIC LATTICE MODEL

By

SHREYA VEMUGANTI

B.E., CIVIL ENGINEERING, OSMANIA UNIVERSITY, INDIA, 2014

M.S., CIVIL ENGINEERING, UNIVERSITY OF NEW MEXICO, USA, 2016

Abstract

Concrete members deform discontinuously in the form of cracks and fracture. Continuum mechanics, which has dominated the field of solid mechanics over the years, does not handle such discontinuities. A material, as defined by continuum mechanics is that which is continuous and fills the space it occupies. Although this is a reasonable assumption for metals, it is an unrealistic notion for concrete.

Stewart Silling invented peridynamics, which involves nonlocal solid modelling upon a continuous material space. Walter Gerstle developed a practical application of the peridynamic model for solid mechanics called the state-based peridynamic lattice model (SPLM). This approach involves material modelling with a finite number of interacting lattice particles rather than a continuum. The advantage of SPLM lies in its ease of computational implementation. SPLM is used in this thesis to analyze the very widely used Brazilian split cylinder test in estimating the uniaxial tensile strength of concrete. Additionally, the direct tension test and the modulus of rupture test are modelled to better understand the tensile strength of concrete and concrete behavior.

Contents

List of figures

List of Tables

Chapter 1 Introduction

1.1 Motivation

Human understanding has evolved over the years. Technological advancements have made it possible to understand and solve increasingly complex problems. Necessity is the mother of invention. The first freely programmable mechanical computer in the world, Z1 was built by Konrad Zuse in 1938 (Rojas, 1997). It was unforeseen then, how computers would dominate technology. But now, computers have become a necessity and have forever changed science and technology.

Understanding the behavior of deformable bodies has gained a lot of attention in the field of design. Though many models already exist, a new model for deformable solids is needed. In this thesis, it is attempted to explain the need for this new model and also describe it with examples. Some of the great engineering minds of the past who used calculus to analyze structural members are Newton, Euler, Bernoulli, Navier, Cauchy, etc. The theories proposed by the latter four involved a set of partial differential equations to solve linear elastic problems. These methods were impractical for direct engineering applications and this gave birth to simplified theories of elasticity to analyze deformable solids. Later, two main categories, namely mechanics of materials and continuum mechanics, were developed.

While mechanics of materials had become the most workable method for the human mind, it was only approximate and limited. Continuum mechanics brought much more generality allowing solutions to nonlinear relations between stress and strain of the material. However, the major drawback in continuum mechanics is that it could not simulate any discontinuity in the solid body. Large deformations were solvable but the fact that these deformations may ultimately lead

to discontinuities was ignored. In concrete members for example, cracks are observed even before load is applied to them, thus making the members discontinuous.

The need for a new material model was acknowledged by Stewart Silling who came up with the concepts of bond-based peridynamics (Silling, 2000). This theory was developed in the year 2000 and improved in the later years to be called the state-based peridynamics (Silling, Epton, Weckner, Xu, & Askari, 2007). Now, we have the state based peridynamic lattice model (SPLM) developed by Walter Herbert Gerstle which assumes that a solid body is composed of discrete and finite number of particles that interact with each other via force functions. SPLM is a promising approach involving computational simulations to evaluate the design strength of concrete structures. The SPLM particle's motion follows Newton's laws.

1.2 Scope of Thesis

Concrete, the most widely used material in construction, is the topic of interest in this thesis. Over the years, concrete structures have become an important part of the infrastructure. An increasing need for efficient structures demands accurate behavior of concrete, as a material. The quality of bond developed between the aggregate and the cement paste is dependent both on the compressive and tensile strength of concrete. Tensile strength has a great role to play in the evaluation of shear resistance in light weight concrete structural members. Crack initiation and propagation in concrete are very closely related to the tensile properties of the material. This affects the appearance, stiffness and damping of the structure (Cornelissen & Reinhardt, 1984).

Thus the study of loading capacity, serviceability and, in the long term, durability of structures requires the knowledge of tensile strength of concrete. The three test methods to evaluate the tensile strength of concrete are

1. the modulus of rupture test
2. the direct tension test
3. the Brazilian split cylinder test.

Among these tests, the Brazilian split cylinder test is widely used. While the results from this test are used as an indirect measure of concrete splitting strength, research proves that this method is a poor indicator of the uniaxial tensile strength of concrete. This thesis presents a detailed study of the behavior of concrete cylinder specimens under the traditional Brazilian split cylinder test method using the concepts of the state-based peridynamic lattice modelling. The other two tests to determine concrete tensile strength which are the modulus of rupture test and the direct tension test are also simulated and the results are studied. These results are then compared to lab results discussed later.

The simplicity of the SPLM is potentially very attractive to practicing engineers. With the SPLM, the engineer has the opportunity to represent with great physical fidelity the behavior of reinforced concrete structures. A parallel particle simulation code called pdQ is used to analyze these models. To perform SPLM simulations and analyze models, the FORTRAN and MATLAB programming languages are used. Using pdQ, the effects of parameters such as elasticity, plasticity, damage, geometrical nonlinear behavior, bond configuration and interaction between different lattice bodies on the strength of concrete are studied. By comparing the simulation results to laboratory results from the tests conducted by Wright (1955) and SAP2000 analysis, both the strengths and the limitations of using the SPLM for such practical purposes are determined.

The aim of this thesis is to offer practical modeling advice for engineers using the SPLM, provide computational timing statistics, investigate the objectivity of the SPLM and discuss

methods for applying the loads and the support conditions. With the concepts of SPLM along with the power of modern computers, it is intended to show that the classical approaches, namely those mentioned in the ACI code, for analyzing reinforced concrete structures may be improved upon.

1.3 Outline of Thesis

This thesis includes seven chapters: Introduction, Theories of Deformation of Solids, State-based Peridynamic Lattice Model, Concrete Uniaxial Tensile Strength, Investigation of the Objectivity of SPLM, SPLM Analysis of Lab Specimens, and Discussion, Conclusions and Future Work.

Chapter Two discusses the theories of deformable solids and describes the models arising from them. This will help in understanding the similarities and differences between these theories and SPLM. An overview of the theory of elasticity, continuum mechanics, and fracture mechanics is given. Also, Silling's and Gerstle's theories of peridynamics are introduced.

Chapter Three is about SPLM in detail, describing the lattice and the particles and their properties. Also described are the elastic, plastic and damage models in SPLM which are used to solve the problems in this thesis.

Chapter Four explains the significance of the tensile strength of concrete. The three tests used to determine the tensile strength of concrete are described. The standard test procedure of the tests are given. Linear elastic analysis of a standard cylinder model is shown using SAP2000. Comments on an Indirect Tensile Test on Concrete Cylinders (Wright, 1955), a paper published in the Magazine of Concrete Research in 1955 is described in this chapter and the results of each of the test methods in the paper are listed.

Chapter Five investigates the objectivity of the SPLM. Aspects like position of steel platens, effect of time dependent analysis on split strength, and interaction between steel and concrete lattice bodies are analyzed.

Chapter Six presents comparison of peak loads between SPLM analysis and laboratory tests of the Brazilian split cylinder test, direct tension test and the modulus of rupture test. Also, the effect of concrete lattice rotation on the peak strength is analyzed.

Chapter Seven presents a summary of analysis and discussion of the simulations conducted along with some conclusions. Scope for future research work is also discussed.

Chapter 2 Theories of Deformation of Solids

In the very beginning, man began to understand the concepts of design and construction with the help of trial and error methods with wood, soil and stone as the basic materials. Later, the quest for a better and safer lifestyle increased and the applications of mathematics got more and more involved in this process. Pioneers in the past had limited computational power and capabilities. This required them to perform hand calculations to solve problems and then apply them realistically in engineering practice. This could be not be done unless the models were simplified enough. Later, modern equipment like calculators, electronic computers and digital computers were developed which eliminated these limitations. This paved the way for new models and theories.

When Newton established the concepts of mass, force, acceleration and simultaneously calculus, many engineering problems had unexpected solutions. A great amount of attention was then given to the study of elastic axial members using this fundamental tool of mathematics. Natural philosophers, such as Euler and the Bernoulli brothers, were able to model elastic and axial members such as beams and columns successfully without including the concepts of stress and strain. The notions of stress and strain was introduced by Cauchy, which today define what we mean by a ‘deformable body’.

This chapter first provides a brief description of some crucial theories and models along with their limitations, and subsequently introduces the modelling concepts of peridynamics.

Firstly, let us see where the classical solid mechanics fails. The fundamental concepts in classical solid mechanics are stress and strain. The traction vector or the stress vector defined only with respect to a point on a particular oriented surface is

$$\boldsymbol{t} \equiv \lim_{\Delta A \to 0} \left(\frac{\Delta \boldsymbol{F}}{\Delta A} \right) \tag{2.1}$$

where $\Delta \boldsymbol{F}$ is the force vector acting upon area ΔA. This is illustrated in Figure. 2.1.

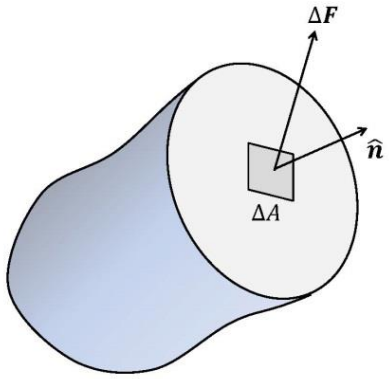

Figure 2.1 Traction vector - from pp.10 (Gerstle, 2015)

For convenience, the vectors are in bold font and the scalars are in normal font. Similarly, the uniaxial normal infinitesimal strain component ε_{xx} also called Cauchy or small-displacement strain is

$$\varepsilon_{XX} \equiv \lim_{\Delta x \to 0} \left(\frac{\Delta u}{\Delta X} \right) = \frac{\partial u}{\partial X}, \tag{2.2}$$

where u is the axial displacement and X is the uniaxial reference position.

As long as the above limits exist to a reasonable approximation, these definitions work fine. The traction vector is defined only when the outward-pointing unit normal $\hat{\boldsymbol{n}}$ is defined uniquely. However, all real materials have microstructure, which means that these limits cannot exist uniquely in any real material. For geometric discontinuities like cracks and corners, these limits do not exist uniquely. So when the displacement field is discontinuous, these definitions are inapplicable.

Consider a typical simply supported beam problem loaded centrally with a point load. When classical linear elastic stress-strain behavior is assumed, an exact closed-form analytical solution to the linear differential equations of elasticity of this problem does not exist. When the solution is expressed as an infinite sum of analytical basis functions, it can be observed that singularities in the stress and strain fields at the supports and the point of loading exist.

In contrast, with SPLM, singularities cannot arise in the solution. Rather than relating stress and strain to interpret material behavior, there exists a constitutive function which relates the *peridynamic discrete deformation state* to the *peridynamic discrete force state*. Thus structural deformations and velocities under mechanical loadings are predicted using SPLM in a simpler way, shedding the stress strain paradigm. In order to appreciate the SPLM, it is important to firstly understand the theory of solid mechanics and its history.

2.1 Theory of Elasticity

The modern theory of elasticity developed over more than four centuries starting with Leonardo da Vinci, Galileo Galilei, Robert Hooke, Isaac Newton, Bernoulli brothers, Euler, Lagrange and Timoshenko. Combined with the concepts of stress and strain, the modern theory of elasticity was first developed in the 1820's by Navier and in the late 1820's by Cauchy.

Navier and Cauchy wrote the pioneering papers about the theory of elasticity in French and this is probably the reason why the basic assumptions they made were misunderstood by many (Gerstle, 2015). These papers have been annotatively translated into English in the book 'Introduction to Practical Peridynamics' written by Gerstle. In this book, the theory is discussed using more familiar notation to modern readers which we will summarize in further sections.

Consider two distinct points $\boldsymbol{P}$ at reference (undeformed) location (X, Y, Z) and $\boldsymbol{P}'$ at a reference location (X', Y, Z') in an elastic body. With respect to the (X, Y, Z) coordinate system, these points are considered to be position vectors. In the non-deformed states, the relative position vector between these two points is given by $\boldsymbol{R} \equiv \boldsymbol{P}' - \boldsymbol{P}$. As the body deforms, points $\boldsymbol{P}$ and $\boldsymbol{P}'$ move to $\boldsymbol{p}$ and $\boldsymbol{p}'$ respectively. Figure 2.2 comprehensively illustrates these states.

The displacement field can be represented using Taylor series expansion as

$$\boldsymbol{U}' \cong \boldsymbol{U} + \frac{\boldsymbol{\partial U}}{\boldsymbol{\partial X}} \boldsymbol{R} \tag{2.3}$$

and the linearized relative displacement vector between **p'** and **p** can be defined as

$$\Delta \boldsymbol{u} = \boldsymbol{U}' - \boldsymbol{U} = \frac{\boldsymbol{\partial U}}{\boldsymbol{\partial X}} \boldsymbol{R} \tag{2.4}$$

The displacement gradient $\frac{\boldsymbol{\partial U}}{\boldsymbol{\partial X}}$, is a tensor and represented as a 3x3 matrix.

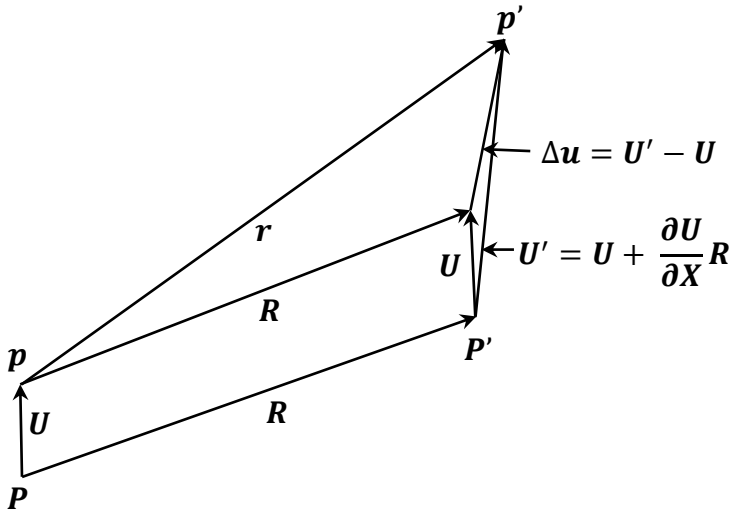

Figure 2.2 Updated representation of Navier theory

There are several important fundamental assumptions which limit the applicability of this theory. Only for displacement vectors $\boldsymbol{u}$ with magnitude much less than $\boldsymbol{R}$, is the linearized relative displacement between two points valid. The magnitude of $\boldsymbol{R}$ must be small compared to the norm of the first derivative to the norm of the second derivative of the displacement field

$$||\mathbf{R}|| \ll \left. ||\frac{\partial \boldsymbol{U}}{\partial \boldsymbol{X}}|| \right/ ||\frac{\partial^2 \boldsymbol{U}}{\partial^2 \boldsymbol{X}}|| \tag{2.5}$$

In addition, the displacement field **U** must be differentiable i.e. continuous. The magnitude, $||\boldsymbol{R}||$ must be such that points $\boldsymbol{P}$ or $\boldsymbol{P'}$ are inside the body. In Navier's model, the change in length ΔR of bond $\boldsymbol{R}$ is given in indicial notation as

$$\Delta R = \frac{(U_{i,k}R_k)R_i}{\sqrt{R_j R_j}} \tag{2.6}$$

Navier then assumes a force-per-unit-volume, F, acting upon $\boldsymbol{P}$. This F corresponds to the volume, dV, associated with particle, $\boldsymbol{P}$, due to the relative displacement of $\boldsymbol{P'}$. F is proportional to the change in length, ΔR, of the bond between the two particles. Considering $G(R)$ to be the rapidly decaying function only of $\boldsymbol{R} = ||\boldsymbol{R}||$ and dV' is the differential volume associated with particle $\boldsymbol{P'}$, F is given by

$$F = G(R)\,\Delta R dV' \tag{2.7}$$

Then by going through a virtual elongation $\delta\Delta R$, the internal virtual work done by each bond is

$$\delta W_{bond} = \delta\Delta R \,.\, F = \frac{1}{2}\,\delta(\Delta R^2)G(R)dV' \tag{2.8}$$

After integration over the entire spatial domain followed by integration in Cartesian and spherical coordinate system, the virtual work per unit volume is obtained in terms of an elastic parameter, ε. Navier assumes body forces, $\boldsymbol{B}$, acting per unit volume, Ω, and surface tractions, $\boldsymbol{T}$, acting per unit boundary surface area, Γ to obtain his final equation of elasticity.

The detailed derivation of this equation can be obtained in (Gerstle, 2015). Navier's equation cannot simulate material with Poisson's ratio other than one quarter since ε is the only elastic parameter in Navier's equation of elasticity which is given by

$$\varepsilon \equiv \left(\frac{2\pi}{15}\right)\int_0^\infty R^4 G(R)dR \tag{2.9}$$

Cauchy showed that Navier's theory was insufficiently general to represent all isotropic linear elastic materials. Therefore, he came up with a model which introduced the concepts of stress and strain. Navier and Cauchy together developed the modern theory of elasticity which was a corrected mathematical formulation involving a set of partial differential equations and relying heavily upon the assumptions of continuity and calculus.

This theory was much more general than to mechanics of materials but was incapable of modelling important features of deformation of solids. Some assumptions related to spatially continuous deformations and small deformations are unrealistic, except in very special conditions. The solutions obtained from this theory are physically unrealistic, involving singularities in stress and strain fields. This led the way to a much more generalized theory of continuum mechanics discussed in the next section.

2.2 Continuum Mechanics

Continuum mechanics is much more generalized than the linear theory of elasticity because the partial differential equations are nonlinear and highly mathematical. The engineering world has been dominated by continuum mechanics over the years. This theory is able to model large deformation problems with nonlinear stress strain relationships. This theory rests on the idea of

the material body being continuous and by assuming continuous spatial, kinematic and kinetic behavior of the materials analyzed. It is essential to include the description of continuum mechanics in this thesis to understand the similarities and differences between the state based peridynamic model, the state based peridynamic lattice model and continuum mechanics.

The roots of continuum mechanics are from Newton's calculus, which rests on the Cartesian coordinate system of real numbers, and N_R-dimensional real Cartesian space denoted by $\mathbb{R}^{N_R}$ invented by Descartes. Since continuum mechanics is mathematically expressed using tensors, we shall define a tensor briefly. An *nth-order tensor* can be defined as a real-valued *m*-linear function of vectors. This implies, an *m*th-order tensor, **T**, is an *m*-linear function that takes *m* vectors in $\mathbb{R}^{N_R}$ and maps them to a real number (Gerstle, 2015). This can be illustrated as

$$\mathbf{T}: \mathbb{R}^{N_R} \times ... \times \mathbb{R}^{N_R} \rightarrow \mathbb{R} \tag{2.10}$$

To understand the basis of continuum mechanics model, the kinematics needs to be studied which is a major part of the continuum mechanics model. Consider the initial spatial position, $\boldsymbol{X}$ of a continuum particle, P. The deformed configuration of this particle, P, is called its current spatial position, $\boldsymbol{x}$. A continuous deformation mapping function, $\boldsymbol{\varphi}$, is used to describe this current spatial position given by

$$\boldsymbol{x} = \boldsymbol{\varphi}(\boldsymbol{X}) \tag{2.11}$$

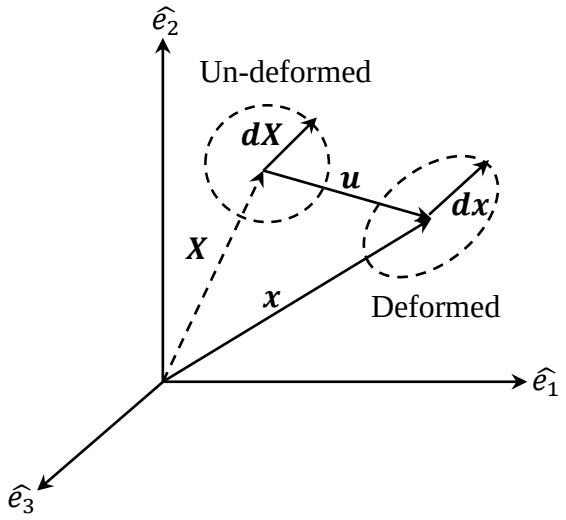

Figure 2.3 Continuum mechanics model

The deformation function, $\boldsymbol{\varphi}$, is a one-to-one bijective because no self-overlap of the body is allowed in deformation and no continuum particle in the initial reference configuration, $\boldsymbol{X}$, can map to two different continuum particles in the deformed configuration, $\boldsymbol{x}$. This implies

$$\boldsymbol{X = \varphi^{-1}(x)} \tag{2.12}$$

Between two initial reference points, $\boldsymbol{X}$ and $\boldsymbol{X'}$, the reference vector is defined as

$$\boldsymbol{dX = X' - X} \tag{2.13}$$

and the spatial vector is defined as

$$\boldsymbol{dx = x' - x} \tag{2.14}$$

The infinitesimal spherical neighborhood of particle, $\boldsymbol{X}$, is deformed into an infinitesimal ellipsoidal neighbourhood of particle, $\boldsymbol{x}$. This gives the mapping, $\boldsymbol{F}$, from $d\boldsymbol{X}$ to $d\boldsymbol{x}$ called the deformation gradient. $\boldsymbol{F}$ is a second order tensor which transforms under the conventional rules of

tensor transformation. This deformation gradient captures at a point, the local spatial rate of deformation. The deformation gradient provides an affine mapping in which parallel lines remain parallel after transformation. This mapping is done in the neighborhood of the particle from un-deformed configuration to the deformed configuration as discussed earlier. $\boldsymbol{F}$ is given by

$$d\boldsymbol{x} = \frac{\partial \boldsymbol{\varphi}}{\partial \boldsymbol{X}} d\boldsymbol{X} = \boldsymbol{F} d\boldsymbol{X} \tag{2.15}$$

In order to define strain, the Cauchy-Green deformation tensor is used as a basis in solid mechanics which is given by

$$\boldsymbol{C} \equiv \boldsymbol{F}^{\boldsymbol{T}} \boldsymbol{F}. \tag{2.16}$$

The Lagrangian strain tensor $\boldsymbol{E}$ is given by

$$\boldsymbol{E} = \frac{1}{2}(\boldsymbol{C} - \boldsymbol{I}) = \frac{1}{2}(\boldsymbol{F}^{T}\boldsymbol{F} - \boldsymbol{I}). \tag{2.17}$$

Similarly, the *Euler-Almansi* strain tensor is given by

$$\boldsymbol{e} = \frac{1}{2}(\boldsymbol{I} - \boldsymbol{B}^{-1}) = \frac{1}{2}(\boldsymbol{I} - \boldsymbol{F}^{-\boldsymbol{T}}\boldsymbol{F}^{-1}). \tag{2.18}$$

$\boldsymbol{I}$ is the identity matrix in the above equations. Both the Lagrangian and the Euler-Almansi strain tensors ($\boldsymbol{E}$ and $\boldsymbol{e}$ respectively) may be linearized with respect to a given configuration, $\boldsymbol{x}$. If they are linearized about the initial reference configuration, the Cauchy small strain tensor, $\boldsymbol{\epsilon}$, can be obtained. After the kinematics of the continuum mechanics model, the physical laws of

mechanics which are related to mass, momentum and thermodynamics may also be applied. For further discussion, refer to (Gerstle, 2015).

Cauchy defined traction, $\boldsymbol{t}$, as the force per unit area in the current configuration. Within a material body, the tractions acting on opposing faces of a planar surface must be equal and opposite. This gives

$$\boldsymbol{t}(\boldsymbol{x}, \boldsymbol{n}) = -\boldsymbol{t}(\boldsymbol{x}, -\boldsymbol{n}), \tag{2.19}$$

where, n, is the unit normal vector shown clearly in Figure 2.1. With this, the Cauchy stress tensor, $\boldsymbol{\sigma}$, which is a second-order tensor, can be obtained as

$$\boldsymbol{t}(\hat{\boldsymbol{n}}) = \boldsymbol{\sigma}.\hat{\boldsymbol{n}}. \tag{2.20}$$

This stress tensor gives the traction vector acting upon a unit area of material in the deformed configuration. The Cauchy stress tensor is divided into two components namely a volumetric component and a deviatoric component. The deviatoric component, $\boldsymbol{s}$, is given by

$$\boldsymbol{s} = \boldsymbol{\sigma} + p\boldsymbol{I}, \tag{2.21}$$

where p, is the pressure, which is the hydrostatic part of the Cauchy stress tensor. p, is given in terms of the trace of a tensor as

$$p = \frac{-tr(\boldsymbol{\sigma})}{3}. \tag{2.22}$$

Defining the first Piola-Kirchoff stress tensor ($\boldsymbol{P}$) and the second Piola-Kirchoff stress tensor ($\boldsymbol{S}$) and the Kirchoff stress tensor ($\boldsymbol{\tau}$), we arrive at an expression which defines the Cauchy stress tensor in terms of the deformation gradient. $\boldsymbol{P}$, $\boldsymbol{S}$, $\boldsymbol{\tau}$ are given by

$$\boldsymbol{P} = \boldsymbol{\tau}\boldsymbol{F}^{-T} \tag{2.23}$$

$$\boldsymbol{S} = \boldsymbol{F}^{-1}\boldsymbol{P} \tag{2.24}$$

$$\boldsymbol{\tau} = det(\boldsymbol{F})\boldsymbol{\sigma} = J\,\boldsymbol{\sigma} \tag{2.25}$$

Therefore, the Cauchy stress tensor is

$$\boldsymbol{\sigma} = \frac{\mathbf{1}}{J}\boldsymbol{F}\boldsymbol{S}\boldsymbol{F}^{T} \tag{2.26}$$

In large-deformation mechanics of continuous bodies, these stress measures are meaningful. However, they are very difficult for a practicing engineer to apply. To obtain the elastic constants for a linear elastic isotropic material, linearized stress strain equation is written in terms of the increment in the second Piola-Kirchoff stress tensor ($d\boldsymbol{S}$), the increment in the Green-Lagrangian strain ($d\boldsymbol{E}$) and the Cauchy-Green deformation tensor ($\boldsymbol{C}$) as

$$dS_{ij} = C_{ijkl}dE_{kl} \tag{2.27}$$

$$C_{ijkl} = \lambda\delta_{ij}\delta_{kl} + \mu\,(\delta_{ik}\delta_{jl} + \delta_{il}\delta_{jk}) \tag{2.28}$$

Here, λ and μ are called Lamé constants. In terms of Young's modulus E and Poisson's ratio ν, the Lamé constants are given by

$$\mu = \frac{E}{2(1+\nu)} \text{ and } \lambda = \frac{\nu E}{(1+\nu)(1-2\nu)} \tag{2.29}$$

The theory of continuum mechanics demands all fields associated with a material body be continuous. This spatially continuous body is fundamentally a collection of discrete particles like atoms, molecules, aggregate, and sand. With the nonlinear partial differential equations, this discipline of continuum mechanics claims to model large deformations and plasticity but this is

complicated and unrealistic. This is because no geometric domain with sharp corners, cracks, and rough boundaries can have a continuous traction vector. Materials do not always deform continuously. Also, these problems may have non-quantitative solutions as sharp corners and cracks permit infinite stresses and strains.

Due to these limitations of both the classical elastic theory and continuum mechanics, fracture mechanics was developed in the early twentieth century.

2.4 Fracture Mechanics

Fracture was not a scientific discipline until the mid-1800s. Industrial advancements and evolution demanded solutions to problems involving fracture and cracking. Fracture was largely ignored by the pioneers of elastic theory. This was probably because calculus was based on smooth and continuous functions and these functions cannot easily describe sharp discontinuities like cracks. In the twentieth century, Charles Edward Inglis (Inglis, 1913) provided the first analytical solution to a problem which was similar to a crack. He showed that for solids with sharp cracks, the traditional stress based approach cannot be allowed to predict load at failure because there exists a singularity in stress. Inglis considered a problem of an infinitely large plane-stress plate having an elliptical hole and subjected to uniaxial tension shown in Fig. 2.4.

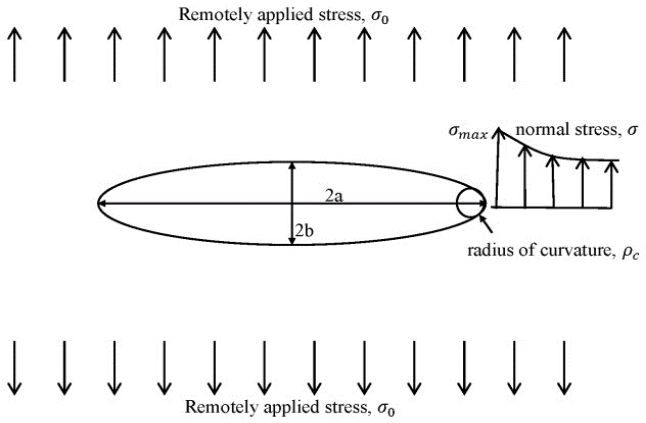

Figure 2.4 Inglis' infinite plate with hole - from pp.121 (Gerstle, 2015)

Inglis showed that the stress within the directly adjacent material on the major axis of the ellipse reaches infinity as the elliptical hole becomes narrow. The maximum tensile stress on the major axis of the elliptical hole is given by

$$\sigma_{max} = \sigma_0 \left(1 + 2 \sqrt{\frac{a}{\rho_c}} \right) \tag{2.30}$$

where, $\rho_c = \frac{b^2}{a}$, is the radius of curvature at the end of the major axis of the ellipse. For an infinitely sharp crack, the ratio, $\frac{\sigma_{max}}{\sigma_0} = \infty$. The stresses at this crack tip for plane strain and plane stress problems were given by Westergaard (Westergaard, 1939) and Williams (Williams, 1997). Through the expressions for stress, stress intensity factors K_I, K_{II}, K_{III} are introduced which correspond to the three modes of deformation namely *opening mode*, *sliding mode* and *tearing mode*. Using these factors, the stress field at points within a singular elastic zone located close to the crack tip can be obtained. However, this is far from the volume of material close to the crack front, within which damage takes place, mostly referred to as a fracture process zone (FPZ).

An energy criterion was brought to the linear elastic fracture mechanics (LEFM) by (Griffith, 1921). He explained first that one must look beyond the theoretical infinite stresses at sharp cracks and corners, to energy, to understand crack propagation. He developed a very important crack propagation criterion called the "Griffith energy criterion" which predicts that when the rate of change of potential energy with respect to the newly formed crack area exceeds a critical value (otherwise called the critical energy G_F), the necessary potential energy needed for the crack to propagate is released. It was proved that this criterion worked well for glass but when accidents involving steel ships breaking into two halves occurred, it was evident that this criterion underestimated the resistance of steel to crack growth and propagation.

Later, Irwin (Irwin, 1957) proposed that a plastic zone exists in the FPZ in steel which absorbs more energy as a crack propagates than what is absorbed as only the surface energy. When the plastic portion of the FPZ is smaller than other dimensions in the problem, it contains a stress field affected by only K_I, K_{II}, K_{III}, otherwise, the problem geometry and loading affect this stress field. Irwin's equation for the critical fracture energy thus includes surface energy and energy of plastic work which is given by

$$G_F = G_{surface} + G_{FPZplasticity}. \tag{2.31}$$

For a symmetrically loaded crack, with distance from crack tip (r) and angle with respect to the plane of the crack (θ), the elastic stress field in the vicinity of the crack tip having Cauchy stress components $\sigma_{ij}(r,\theta)$ and simple trigonometric functions f_{ij} is given by

$$\sigma_{ij}(r,\theta) = \frac{K_I}{\sqrt{2\pi r}}\, f_{ij}(\theta) \tag{2.32}$$

The energy release rate *G* for a planar crack growth is

$$G = \frac{K_I^2}{E'} + \frac{K_{II}^2}{E'} + \frac{K_{III}^2}{2\mu}, \tag{2.33}$$

for plane stress,
$$E' = E, \tag{2.34}$$

for plane strain,
$$E' = \frac{E}{1 - \nu^2}, \tag{2.35}$$

and
$$\mu = \frac{E}{2(1 + \nu)}, \tag{2.36}$$

where E is the Young's modulus, ν is the Poisson's ratio and μ is the shear modulus.

Equation 2.32 is not valid in three-dimensional crack problems where the stress intensity factors may vary along the crack front. Also, with mode II crack growth, the crack changes direction. Irwin then came up with stress intensity factor called fracture toughness K_{IC} at which a plane-strain Mode I crack begins to propagate. But this factor also has a lot of limitations.

Thus LEFM only works for specific situations and problems. The linear elastic theory of fracture mechanics allows prediction of the propagation of cracks by modifying the geometry of the domain with the help of finite element methods or boundary element methods. These cracks thus propagate and the point of nucleation of these cracks along with its trajectory is determined by the theory of fracture mechanics. This process is not simple. It is not easy to modify the

geometry and boundary conditions in a consistent manner using finite element meshes unless simplifying assumptions are made. The traditional linear elastic fracture mechanics concept considers a crack to be a surface of separation with no tractions between the newly developed crack surfaces. This is not completely true. The theory is insufficient in conditions where plasticity enters the regime of propagating cracks.

This led to the development of nonlinear fracture mechanics which proposed the concepts of fictitious crack models called nonlinear fracture mechanics models. These models could not be solved analytically and required computational models to solve for at least approximate solutions. This gave birth to the computational fracture mechanics. There were three methods included in this approach (Gerstle, 2015). They were,

1. Discrete crack models
2. Smeared crack models
3. Lattice and particle models.

While the smeared crack models have been widely used to predict the nonlinear behavior of concrete structures, lattice models have been more specific in modelling materials at the meso-scale level and more complex than macro-scale behavior.

A more fundamental approach to fracture mechanics was then proposed by Silling (2000), who developed the peridynamic model. Peridynamic modelling is introduced along with the bond-bond based peridynamic model and the state-based peridynamic model in the following sections.

2.5 Peridynamics

Peridynamics, developed by Stewart Silling (Silling, 2000), is a coherent alternative framework to the Cauchy stress strain theory. Peridynamics is derived from the Greek roots '*peri*' which means near and '*dynamic*' which means force. The first theory of peridynamics was the bond-based peridynamic theory. This original continuum peridynamic model is based on the assumption that Newton's second law is true for every infinitesimal particle within the domain of analysis (Gerstle, 2015; Silling, 2000). In this theory the force between any two particles is assumed to be a function of only the states of the two particles. This force is referred to as a peridynamic kernel or a force density function also known as the pairwise force function having units of force per unit volume per unit volume. The pairwise force function is not dependent on nearby particles' states.

When the bond-based theory was found to be insufficiently general to model some known behaviors of real materials, Silling introduced the state-based peridynamic theory in (Silling et al., 2007). Both bond-based and state-based peridynamic theories rest on the concepts of continuum mechanics assuming material to be spatially continuous.

Later, to include the concepts of peridynamic particle moments and rotations, micropolar peridynamic theory was introduced (Gerstle, Sau, & Silling, 2007). This theory had much more advantages when compared to the bond-based theory but was quite complicated when large rotations were involved. In light of these difficulties, Gerstle introduced the state-based peridynamic lattice model shedding entirely the assumptions of spatial material continuity. In this theory, rather than an infinite number of continuum particles, a material is modelled as a finite

number of lattice particles interacting with each other. A state based peridynamic lattice model is adopted in the current thesis.

2.6 Bond-based Peridynamic Theory

To understand the kinematics of the bond based continuum peridynamics, consider a particle, *P*, at undeformed location, $\boldsymbol{X}$, which deforms to location, $\boldsymbol{x}$, under an applied load. Similarly, consider a particle, *P'*, at undeformed location, $\boldsymbol{X'}$, which deforms to a location, $\boldsymbol{x'}$. The displacement vector of particle *P* is $\boldsymbol{u} = \boldsymbol{x} - \boldsymbol{X}$ and the displacement vector of *P'* is $\boldsymbol{u'} = \boldsymbol{x'} - \boldsymbol{X'}$. The vector from $\boldsymbol{X}$ to $\boldsymbol{X'}$ in Figure 2.5, is defined as the reference bond $\boldsymbol{\xi}$. The

deformed configuration of the reference bond or otherwise the image of $\boldsymbol{\xi}$ is called the deformed bond, $\boldsymbol{\xi} + \boldsymbol{\eta}$. The basic assumption in bond-based theory is that the force between *P* and *P'* depends only on $\boldsymbol{\xi}$ and $\boldsymbol{\xi} + \boldsymbol{\eta}$, the reference and the deformed bonds respectively.

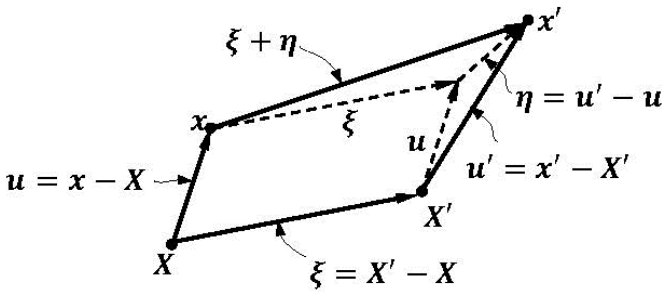

Figure 2.5 Kinematics in bond-based peridynamic theory – from pp149 (Gerstle, 2015)

The vector-valued function, $\boldsymbol{f}$, is the interactive force between particles at $\boldsymbol{X}$ and $\boldsymbol{X'}$. $\boldsymbol{f}$, is a function of the undeformed bond and the deformed bond of the two particles. The particles at $\boldsymbol{X}$ and $\boldsymbol{X'}$ interact only if they are 'close enough'. This finite distance is referred as the material horizon radius, $\boldsymbol{\delta}$. Function $\boldsymbol{f}$ is given by

$$\boldsymbol{f}(\boldsymbol{\eta},\boldsymbol{\xi}) = \mathbf{0}, \forall\, \boldsymbol{\eta}, \forall \left|\left|\boldsymbol{\xi}\right|\right| > \boldsymbol{\delta} \tag{2.37}$$

2.7 Pairwise Force Function

Consider the force acting on particle, P, located at undeformed position, $\boldsymbol{X}$. At any time t, this force per unit volume, $\boldsymbol{L_u}$, is given as the sum of infinitesimal pairwise forces acting on P given by

$$\boldsymbol{L_u}(\boldsymbol{X}) = \int_{\mathcal{R}} \boldsymbol{f}(\boldsymbol{u}' - \boldsymbol{u}, \boldsymbol{X}' - \boldsymbol{X}) dV', \;\; on\, \mathcal{R} \tag{2.38}$$

Say, particle P has differential mass $dm = \rho_0 dV \equiv \rho_0 dV(X)$ where, ρ_0, is the mass-per-unit-reference-volume. Applying Newton's second law to P,

$$dm\ddot{\boldsymbol{u}} = \rho_0 dV \ddot{u} = (\boldsymbol{L_u} + \boldsymbol{b}) dV, \;\; on\, \mathcal{R} \tag{2.39}$$

where the externally applied body force-per-unit-reference-volume is $\boldsymbol{b}$ and $\mathcal{R}$ is the reference space assumed to be a subset of a real three-dimensional Cartesian space, $\mathbb{R}^3$. Finally,

$$\rho_0 \ddot{\boldsymbol{u}} = \int_{\mathcal{R}} \boldsymbol{f}(\boldsymbol{u}' - \boldsymbol{u}, \boldsymbol{X}' - \boldsymbol{X}) dV' + \boldsymbol{b}, \;\; on\, \mathcal{R} \tag{2.40}$$

where $\boldsymbol{f}(\boldsymbol{u}' - \boldsymbol{u}, \boldsymbol{X}' - \boldsymbol{X}) = \boldsymbol{f}(\boldsymbol{\eta}, \boldsymbol{\xi})$, is called the pairwise force function with units of force-per-(volume squared). Density and body force are concepts dependent on continuity of the mass distribution and of the reference space, $\mathcal{R}$. For simplicity, the reference space is assumed to be a homogeneous, single material. If $\boldsymbol{f} > limiting\ value$, then peridynamic micro-damage, ω, can occur. This will cause $\boldsymbol{f}$ to decrease with increasing bond stretch and discontinuities may form in the deformation field. This ultimately leads to a crack or fracture. Thus the peridynamic model has the ability to model continuous behavior, damage and fracture in a unified computational framework (Gerstle, 2015).

$\boldsymbol{f}$, need not be a smooth function, but it has a few restrictions. $\boldsymbol{f}$, must satisfy Newton's third law and also the conservation of angular momentum. This theory required that the forces between a pair of particles are not only functions of the reference and deformed locations but also equal, opposite and collinear with deformed locations of the two particles. This can be represented as shown in Fig. 2.6.

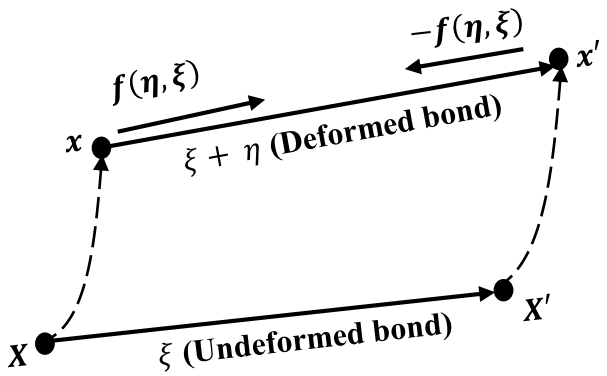

Figure 2.6 Pairwise force function $\boldsymbol{f}$

The bond-based model is insufficiently general to model materials with Poisson's ratio other than one-quarter. As a result, the bond-based micropolar peridynamic model was introduced which included peridynamic particle moments and rotations. The advantages of this model were that materials with varying Poisson's ratio could be modeled and also complex material behavior could be modeled. It was also possible with this model to simulate reinforcement with behavior such as bending and shear and also a single line of particles. This model however becomes complicated for large rotations. Due to all these difficulties, the state based peridynamic theory was introduced.

2.8 State-based Peridynamic Theory

The state-based peridynamic theory was introduced as an extension to the bond-based peridynamic theory by including the concepts of *force state* $\underline{\boldsymbol{T}}$ and *deformation state* $\underline{\boldsymbol{Y}}$. This theory allows the pairwise force function between two particles, P and P', to be a function of the relative reference position, $\boldsymbol{\xi}$, and the relative displacement, $\boldsymbol{\eta}$, as well as the reference and deformed positions, $\boldsymbol{X}$ and $\boldsymbol{x}$, of all particles that are within the union of material horizons of both particles P and P'.

The state-based peridynamic theory is more general than continuum mechanics. Linear elastic materials with varying Poisson's ratio can be modelled using this theory. Additionally, rate dependent analysis can also be included. It is capable to represent continuous and discontinuous deformations and also dynamic behavior of materials. While all these generalizations exist, it is still unclear how the discontinuous fields can be represented on the computer in a simple way. The state-based peridynamic theory is explained in Chapter 3.

Chapter 3 State Based Peridynamic Lattice Model (SPLM)

3.1 Introduction

The state-based peridynamic lattice model (SPLM) was introduced by Gerstle and his students in which, rather than an infinite number of continuum particles, the material is modelled as a finite number of interacting lattice particles. This is a specialization of Silling's continuum peridynamic model. The problem of defining mass density can be avoided by employing a lattice particle. The interaction of these particles with a specified mass is done by way of peridynamic-bond forces interacting with neighboring particles. It is assumed that these forces are a function of bond stretches of all neighboring particles. The SPLM is combined with powerful computers to solve problems in solid mechanics.

Prior to moving on to the SPLM, Gerstle noted that neither the bond-based peridynamic lattice model nor the micropolar lattice model was promising to implement isochoric plasticity (Gerstle, 2015). In this chapter, we will describe briefly the key concepts of the SPLM which will enable the reader to understand the simulations performed in the next chapters. In order to understand the SPLM, it is first important to study the discretization of the material body. Later on, we will study lattice particles and the peridynamic lattice models for elasticity, damage, plasticity.

3.2 Lattice Model and Particles

3.2.1 The Lattice $\mathcal{L}$

In order to obtain a computational solution, the system needs to be discretized. With the bond-based theory, general material behavior cannot be modelled. Both the bond-based and the state-based peridynamic theories rest on the concepts of continuum mechanics. This means that the constitutive model has infinite number of points and at all of these points, $\rho_0 \ddot{\boldsymbol{u}} = \int_{\mathcal{R}} \boldsymbol{f}(\boldsymbol{u}' - \boldsymbol{u}, \boldsymbol{X}' - \boldsymbol{X}) dV' + \boldsymbol{b}, \ on \ \mathcal{R}$ must be satisfied. Thus, the system of equations need discretization in order to be implemented on a modern computer (Gerstle, 2015). To discretize the model, geometry of the solid body may be represented as a lattice of material particles instead of a continuum.

The motion of this material body is described using four methods according to (Truesdell, 1965). To apply Newton's laws and implement them on digital computers, we will use the natural *material* description unlike in continuum mechanics which uses the *relative*, *spatial* or the *referential* description as the independent variable. Thus, position is defined as $\boldsymbol{x} = \boldsymbol{x}(P, t)$ and velocity is defined as $\boldsymbol{v} = \boldsymbol{v}(P, t)$ where, the independent variables describing the domain of $\boldsymbol{x}, \boldsymbol{v}$ are P, t. Note that P is the name of a particle and not the position of a particle.

There are several reasons for using a lattice to represent a solid body. Simplicity is one of them. Also, in a finite-mass-particle-based-model, mass is conserved by virtue of the fact that the mass of particle does not vary with time. Momentum is conserved by applying Newton's second and third laws appropriately to a particle. Conservation of energy is achieved by selecting appropriate peridynamic and thermodynamic particle interactions. Symmetry can be exploited by

adopting a lattice. In a lattice, each particle occupies an identical volume. Several other advantages of lattices are found in (Gerstle, 2015).

3.2.2 Lattice Topology, Material Neighborhood, Domain Discretization

Topology, material neighborhood and domain discretization are significant in the study of peridynamic lattices. The study of connectivity is referred to as topology. Questions like nearest neighbor to a certain particle, second nearest neighbors to that particle and so on can be answered with the help of lattice topology. Lattice topology also gives an organized bond structure to a particle and its neighbors such that the constitutive model of SPLM can be easily represented. Lattice topology is also useful to understand whether a particle is on the boundary of a lattice body or not. We can also identify numbering of bonds with lattice topology which is introduced in the next section. In order to simplify the identification of the nearest neighbor to a point, we will consider the topology of an integer metric space.

The set of points with which each material particle interacts within the solid body is called the neighborhood of the particle. If the particle domain has N_P particles then, the number of force interactions per time step is $N_F = \frac{N_P(N_P-1)}{2} = \frac{{N_P}^2}{2}$. This is for a large number of particles. In order to reduce the number of force interactions, the domain can be decomposed into an array of cubical cells whose size is greater than the peridynamic horizon δ. Now the force interactions of a particle are only with particles within its own cell ($N_Q \approx 18$) and particles within adjacent cells ($N_A \approx 27$) and $N_F \approx \frac{N_P \times N_A \times N_Q}{2}$. Thus the number of force interactions are reduced with domain decomposition. To avoid domain decomposition, a neighbor list which defines the topology of discrete particles can be precomputed before entering the time integration loop which will be discussed later.

3.2.3 Mathematical Description of a Particle Lattice Model

A regular rectangular, hexagonal close packed (HCP) or face-centered cubic (FCC) array of particles are shown in Fig. 3.1. The layers of an FCC packing step constantly. Refer to definitions 6.2 and 6.3 in Gerstle (2015). For a one dimensional problem, a straight row of equally spaced particles can be assumed. For a two dimensional problem, a close packed hexagonal lattice and for a three dimensional problem, a face-centered cubic lattice can be assumed.

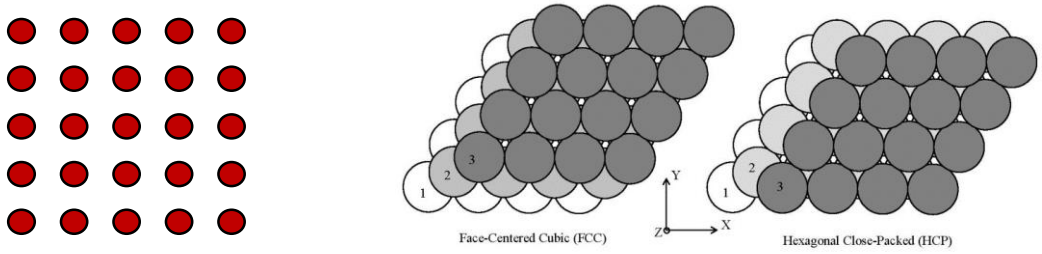

(a) **(b)**

Figure 3.1 (a) Rectangular array (b) Face centered cubic array and Hexagonal array – from pp187. (Gerstle, 2015)

Lattice Λ^{N_R} contains an infinite number of lattice points. The lattice coordinates are given by $N_R \times 1$ array of integer components $\{a_i\}$ with respect to a lattice basis, B^{N_R}. The important parameters needed to describe a lattice mathematically are given in Table. 3.1.

Table 3.1 Lattice related notations

$\mathbb{Z}^3$	3D integer space
$\mathbb{R}^3$	3D Real Euclidian space
$\mathbb{R}^{N_R}$	N_R-dimensional real Euclidian space
$\boldsymbol{X} = \sum_{i=1}^{N_R} X_i \hat{\boldsymbol{e}}_{\boldsymbol{i}}$	Initial reference location of particle *P*
$\hat{\boldsymbol{e}}_{\boldsymbol{i}}$	Unit basis vector
$\{X_i\}$	Array of initial, undeformed coordinates
$\boldsymbol{X_0}$	Location of origin of lattice coordinates
B^{N_R}	Lattice basis with a set of N_R-dimensional vectors $\boldsymbol{b}_{\boldsymbol{i}}$
$B^{N_R} = \{\boldsymbol{b_1} \dots \boldsymbol{b}_{\boldsymbol{N_R}}\}$	A set of $\boldsymbol{b}_{\boldsymbol{i}} \in \mathbb{R}^{N_R}$
$[B^{N_R}] = \begin{bmatrix} b_{11} & \cdots & b_{N_R{}^1} \\ \vdots & \ddots & \vdots \\ b_{1N_R} & \cdots & b_{N_R N_R} \end{bmatrix}$	Lattice basis matrix
Λ^{N_R}	N_R-dimensional lattice in $\mathbb{R}^{N_R}$
Λ	Lattice when N_R is unimportant
$\mathcal{L}_{\mathcal{R}}$	Lattice body-subset of the particles within $\mathcal{R}$
$\mathcal{R}$	N_R-dimensional solid body in $\mathbb{R}^{N_R}$
$\mathrm{d}(\Lambda^{N_R}) = det[B^{N_R}]$	*Co-volume* of a lattice

A material in a linear elastic regime is represented by two properties namely modulus of elasticity *E* and Poisson's ratio ν. In SPLM another property called lattice spacing *L* is introduced. For each material body, a material lattice provides a length scale *L*. This is helpful in constitutive modeling as it specifies the level of detail of the material body. This scale should not be smaller

than the intrinsic length scale of a material. The only restriction on the particle mass is that the lattice spacing cannot be smaller than the largest component of the meso material. This is why a lower limit is set on the lattice spacing for solid modeling in SPLM.

3.2.4 Bond and Particle Bond List

Bond is defined as the potential interaction of a particle $P_i \in \Lambda$, with other particles. For a single typical particle in FCC particle lattice with lattice particle spacing L, and a rigid body rotation matrix $[Q]$, the lattice basis matrix is given by

$$[B^3] = L[Q]\begin{bmatrix} 1 & \frac{1}{2} & \frac{1}{2} \\ 0 & \frac{\sqrt{3}}{2} & \frac{1}{2\sqrt{3}} \\ 0 & 0 & \sqrt{\frac{2}{3}} \end{bmatrix} \tag{3.1}$$

A sequential list with all the bonds between a particle and other potentially interacting particles in the lattice is called a lattice *particle bond list* $\mathbb{B}$. The numbering is done as sequential integers from 1 to the number of bonds per particle, N_B (refer to Definition 6.6 in (Gerstle, 2015)). P_i's neighbor list $\mathcal{N}[P_i]$ maps the particle bond list to adjacent lattice particles,

$$\mathcal{N}[P_i]\langle\cdot\rangle\colon \mathbb{B} \longrightarrow \mathbb{P} \tag{3.2}$$

If there is no adjacent particle for P_i, then

$$\mathcal{N}[P_i]\langle B_j\rangle = P_\emptyset \tag{3.3}$$

where $P_\emptyset$, is a null particle of $\mathbb{P}$. The numbering and positioning of the bonds, B_j, for a single particle in FCC lattice is shown in Fig. 3.2.

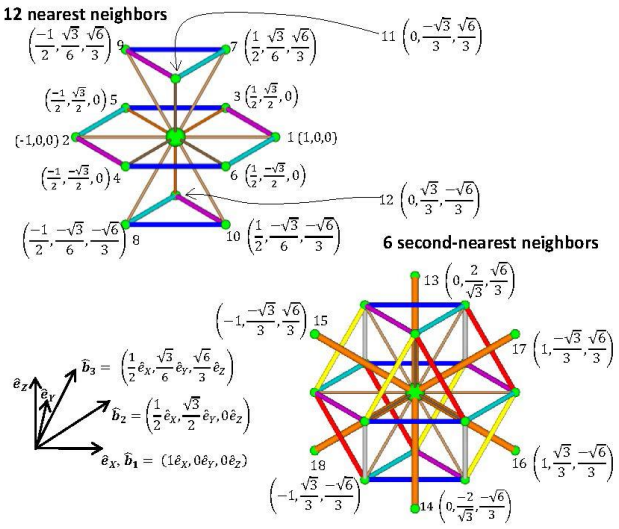

Figure 3.2 Bond numbering order and reference coordinates of first and second nearest neighboring particles for FCC lattice – from pp191. (Gerstle, 2015)

The twelve nearest neighbors are of an undeformed length, L, and the six second-nearest neighbors are of undeformed length, $\sqrt{2L}$. The reference coordinates, $\boldsymbol{X}$, of the corresponding bond number are listed in Table 3.2

Table 3.2 Reference coordinates

Bond Number	**(X,Y,Z)**	**Bond Number**	**(X,Y,Z)**
1	(1,0,0)	10	$\left(\frac{1}{2},\frac{-\sqrt{3}}{6},\frac{-\sqrt{6}}{3}\right)$
2	$(-1,0,0)$	11	$\left(0,\frac{-\sqrt{3}}{3},\frac{\sqrt{6}}{3}\right)$
3	$\left(\frac{1}{2},\frac{\sqrt{3}}{2},0\right)$	12	$\left(0,\frac{\sqrt{3}}{3},\frac{-\sqrt{6}}{3}\right)$
4	$\left(\frac{-1}{2},\frac{-\sqrt{3}}{2},0\right)$	13	$\left(0,\frac{2}{\sqrt{3}},\frac{\sqrt{6}}{3}\right)$
5	$\left(\frac{-1}{2},\frac{\sqrt{3}}{2},0\right)$	14	$\left(0,\frac{-2}{\sqrt{3}},\frac{-\sqrt{6}}{3}\right)$
6	$\left(\frac{1}{2},\frac{-\sqrt{3}}{2},0\right)$	15	$\left(-1,\frac{-\sqrt{3}}{3},\frac{\sqrt{6}}{3}\right)$
7	$\left(\frac{1}{2},\frac{\sqrt{3}}{6},\frac{\sqrt{6}}{3}\right)$	16	$\left(1,\frac{\sqrt{3}}{3},\frac{-\sqrt{6}}{3}\right)$
8	$\left(\frac{-1}{2},\frac{-\sqrt{3}}{6},\frac{-\sqrt{6}}{3}\right)$	17	$\left(1,\frac{-\sqrt{3}}{3},\frac{\sqrt{6}}{3}\right)$
9	$\left(\frac{-1}{2},\frac{\sqrt{3}}{6},\frac{\sqrt{6}}{3}\right)$	18	$\left(-1,\frac{\sqrt{3}}{3},\frac{-\sqrt{6}}{3}\right)$

3.2.5 Lattice Model for a Deformable Solid Structure

The definitions of a structure, a material body, a material particle and its attributes are represented in Fig. 3.3. A structure has component lattice bodies which are of different materials. A material body consists of a lattice body, a particle list, a bond list, and a neighbor list. A material particle is characterized by *particle fixed attributes* and *particle alterable attributes*.

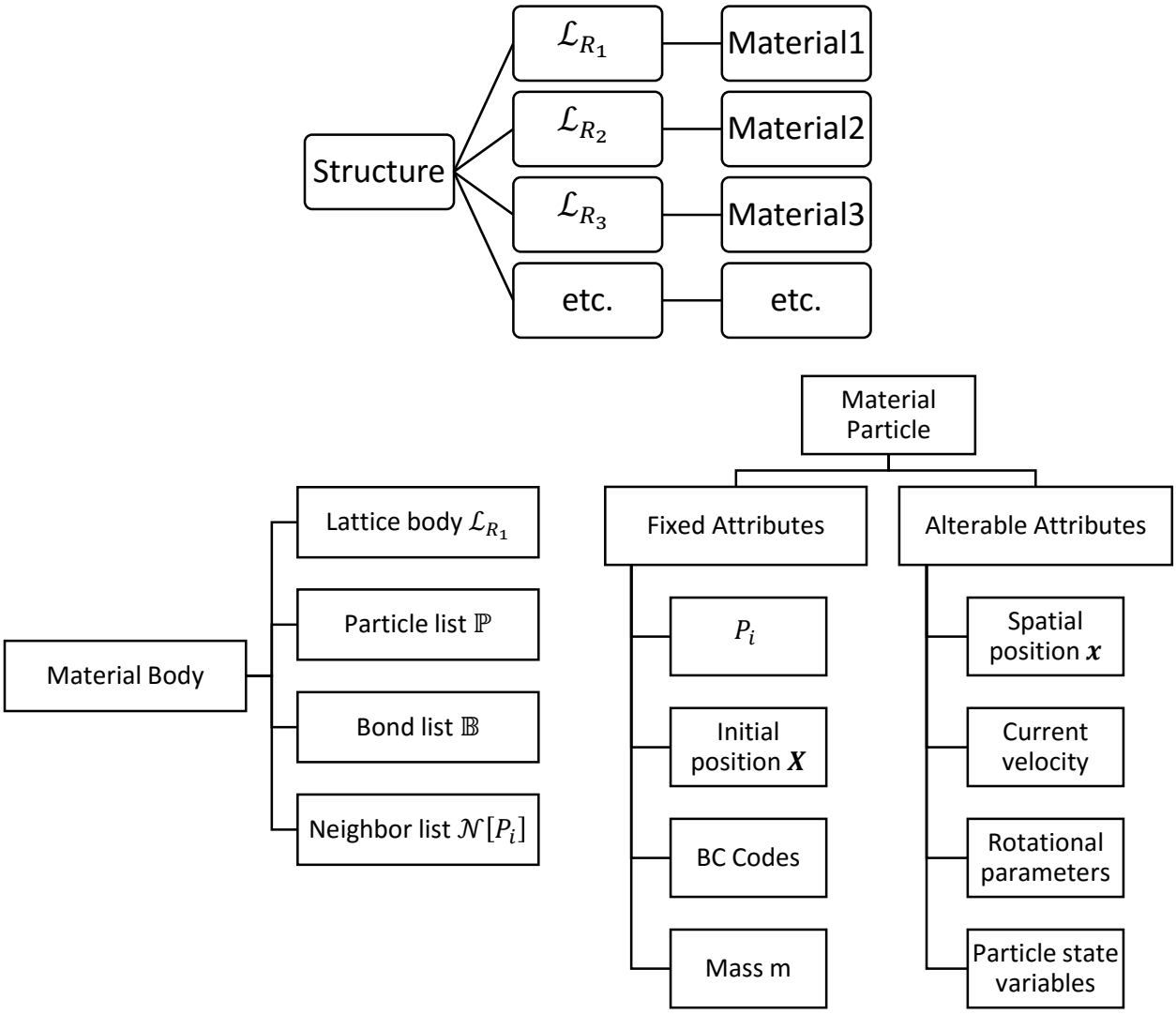

Figure 3.3 Charts representing a deformable solid structure

3.3 State-based Peridynamic Lattice Model (SPLM)

In this section, we describe the state-based peridynamic theory and the state-based peridynamic lattice model. As discussed earlier, the state-based peridynamic theory was introduced as an extension to the bond-based peridynamic theory by including the concepts of *force state* $\underline{\boldsymbol{T}}$ and *deformation state* $\underline{\boldsymbol{Y}}$. The pairwise force function between two particles, P and P', is not only a function of the relative reference position, $\boldsymbol{\xi}$, and the relative displacement, $\boldsymbol{\eta}$, but also a function of the reference and deformed positions, $\boldsymbol{X}$ and $\boldsymbol{x}$, of all particles that are within the union of material horizons of both particles P and P'.

A bond-based state is defined in definition 8.1 (Gerstle, 2015). Basically a bond-based state is a tensor field defined upon a domain. Table 3.3 compares the parameters from Silling's state-based peridynamic theory and Gerstle's state-based peridynamic lattice model.

Table 3.3 Bond-based peridynamic theory vs state-based peridynamic lattice model

'Bond-based state' based Peridynamic Theory	**'State'-based Peridynamic Lattice Model**
Particle P is an element of a continuous subset $\mathcal{R}$	Particle P is an element of a lattice body $\mathcal{L}_{\mathcal{R}}$
$\mathcal{R}$ is defined upon $\mathbb{R}^3$	$\mathcal{L}_{\mathcal{R}}$ is defined upon Λ^{N_R}
Domain of the state $\mathcal{H}$	Domain of the state $\mathbb{B}$

In the state-based theory, tools called *reduction* and *expansion* were introduced. Reduction is approximating a vector state with a second-order tensor and expansion is expanding a second-order tensor to a vector state (Gerstle, 2015). In other words, stress to a force state and strain to a deformation state. It is better to avoid this approximation as it can cause loss of information.

The application of Newton's second law in the (bond-based) state based peridynamic theory is represented as

$$m\ddot{\boldsymbol{x}}(P_i, t) = \sum_{\mathbb{B}} \{\underline{\boldsymbol{T}}[P_i, t]\langle B_j\rangle - \underline{\boldsymbol{T}}[P_i, t]\langle B_j'\rangle\} + \boldsymbol{b}(P_i, t), \tag{3.4}$$

The relation that provides values for the force vector state field in terms of the deformation vector state field is the state based constitutive model represented as

$$\underline{\boldsymbol{T}} = \underline{\widetilde{\boldsymbol{T}}}(\underline{\boldsymbol{X_R}}, \underline{\boldsymbol{x_R}}, \Lambda_0) \tag{3.5}$$

where, $\underline{\widetilde{\boldsymbol{T}}}$ is a vector state-valued function of a vector state, and Λ_0 represents all variables except current and reference deformation states. We use constitutive models suited directly to the SPLM to solve some practical problems in this thesis.

3.4 Elastic Model

The *linear elastic model* in SPLM is actually a *non-linear model* in the overall sense because the large deformation bond stretches are non-linearly related to spatial positions. Unlike Navier-Cauchy's linear elasticity, the statically applied forces in SPLM are not linearly related to particle displacements. For full explanation, refer to (Gerstle, 2015). The relation between the lattice-based stretch matrix $\{S\}$ and the lattice-based force matrix $\{T\}$ is linear given by

$$\{T\} = [K]\{S\} \tag{3.6}$$

where $[K]$ is the stiffness matrix, a crucial parameter which will enable SPLM to simulate a classical elastic continuum and simulate the SPLM as a two-parameter model. The stretch matrix associated with particle P_i is

$$\{S\} = \begin{Bmatrix} S_1 \\ . \\ . \\ S_j \\ . \\ . \\ S_{18} \end{Bmatrix}_i , \tag{3.7}$$

where, S_j represents the stretch of an individual bond B_j given by

$$S_j = \frac{L^* - L_0}{L_0}, \tag{3.8}$$

where,

$$L_0 \equiv \sqrt{(X_j - X_i)^2 + (Y_j - Y_i)^2 + (Z_j - Z_i)^2}\,, \tag{3.9}$$

$$L^* \equiv \sqrt{(x_j - x_i)^2 + (y_j - y_i)^2 + (z_j - z_i)^2}, \tag{3.10}$$

where, L_0 is the length of the bond in the reference configuration between particle i, j, and $L^*$is the bond length in deformed configuration.

The force matrix $\{T\}$ associated with particle P_i is one-half of the vector of peridynamic force magnitudes $\{F_j\}_i$, acting in the reference bond direction $\{n_S\}$ or spatial bond direction $\{n_L\}$ directed away from particle P_i.

$$\{T\}_i = \frac{1}{2}\begin{Bmatrix} F_1 \\ . \\ . \\ F_j \\ . \\ . \\ F_{18} \end{Bmatrix}_i . \tag{3.11}$$

The information provided by the deformation state in the state-based peridynamic theory is the same as what the stretch matrix provides and the information provided by the force state in the state-based peridynamic theory is the same as what the force matrix provides. Next, strain matrix and stress matrix can be represented as

$$\{\boldsymbol{\varepsilon}\} = \begin{Bmatrix} \varepsilon_{XX} \\ \varepsilon_{YY} \\ \gamma_{XY} \\ \varepsilon_{ZZ} \\ \gamma_{YZ} \\ \gamma_{XZ} \end{Bmatrix} \text{ and } \{\boldsymbol{\sigma}\} = \begin{Bmatrix} \sigma_{XX} \\ \sigma_{YY} \\ \tau_{XY} \\ \sigma_{ZZ} \\ \tau_{YZ} \\ \tau_{XZ} \end{Bmatrix}. \tag{3.12}$$

To map the classical small strain matrix to the SPLM stretch matrix, [N] is defined as an 18 x 1 matrix for a 3D particle which has eighteen links in an FCC close-packed lattice. The stretch matrix takes into account both elastic and plastic deformations,

$$\{S\} = [N]\,\{\varepsilon\} \tag{3.13}$$

$$\{S\} = \{S^e\} + \{S^p\} \tag{3.14}$$

Finally, to obtain a relation between SPLM force matrix $\{T\}$ and the classical stress matrix $\{\sigma\}$, it is established that the internal virtual work under kinematically equivalent virtual deformations of both classical and SPLM models are equal

$$\delta W_{classical} = \delta W_{SPLM}, \tag{3.15}$$

where
$$\delta W_{classical} = \lfloor\sigma\rfloor\{\delta\varepsilon\}\Delta V \tag{3.16}$$

and
$$\delta W_{SPLM} = \lfloor F\rfloor\left(\frac{L_i}{2}\right)\{\delta S\}. \tag{3.17}$$

Hence, we obtain

$$\lfloor\sigma\rfloor\{\delta\varepsilon\}\Delta V = \lfloor F\rfloor\left(\frac{L_i}{2}\right)\{\delta S\}. \tag{3.18}$$

$\{F\}$ and $\{\sigma\}$ are linearly related as

$$\{\sigma\} = [\mathrm{M}]\,\{F\} \tag{3.19}$$

where
$$[\mathrm{M}] = \frac{1}{2\Delta V}[N]^T[L_i]. \tag{3.20}$$

Volume per particle is given by the co-volume $d(\Lambda^{N_R})$ as

$$\Delta V = d(\Lambda^3) = \frac{L^3}{\sqrt{2}} \tag{3.21}$$

For the linear elastic state based peridynamic lattice constitutive model, a *micro-elastic SPLM stiffness matrix* $[K]$ is assumed as

$$[K] = \begin{bmatrix} \begin{bmatrix} a+b & b & \cdots & b \\ b & a+b & \cdots & b \\ \vdots & \vdots & \ddots & \vdots \\ b & b & \cdots & a+b \end{bmatrix} & [0] \\ [0] & \begin{bmatrix} c & 0 & \cdots & 0 \\ 0 & c & \cdots & \vdots \\ \vdots & \vdots & \ddots & 0 \\ 0 & 0 & 0 & c \end{bmatrix} \end{bmatrix}. \tag{3.22}$$

A classical constitutive matrix $[D]$ is

$$[D] = [M][K][N], \text{ where} \tag{3.23}$$

$$[D] = \frac{E}{(1+\nu)(1-2\nu)}\begin{bmatrix} (1-\nu) & \nu & 0 & \nu & 0 & 0 \\ \nu & (1-\nu) & 0 & \nu & 0 & 0 \\ 0 & 0 & \frac{(1-2\nu)}{2} & 0 & 0 & 0 \\ \nu & \nu & 0 & (1-\nu) & 0 & 0 \\ 0 & 0 & 0 & 0 & \frac{(1-2\nu)}{2} & 0 \\ 0 & 0 & 0 & 0 & 0 & \frac{(1-2\nu)}{2} \end{bmatrix}. \tag{3.24}$$

Solving $[D] = [M][K][N]$,

a, b *and* c are obtained as

$$a = \frac{EL^2}{\sqrt{2}(1+\nu)}, \tag{3.25}$$

$$b = \frac{\sqrt{2}EL^2(1-4\nu)}{32(2\nu-1)(1+\ \nu)}, and \tag{3.26}$$

$$c = \frac{EL^2}{4(1+\nu)}. \tag{3.27}$$

For plane stress,

$$a = \frac{2ELt_b}{\sqrt{3}(1+\nu)}, \tag{3.28}$$

$$b = \frac{2ELt_b\ (1-3\nu)}{6\sqrt{3}(\nu^2-1)}. \tag{3.29}$$

(3.30)

For plane strain,

$$a = \frac{2ELt_b}{\sqrt{3}(1+\nu)}, and$$

$$b = \frac{2ELt_b\,(1-4\nu)}{6\sqrt{3}(2\nu-1)(1+\ \nu)}. \tag{3.31}$$

where t_b is the thickness of the problem. Derivations can be found in (Gerstle, 2015).

3.5 Plastic Model

When a load is applied to a solid body, it is not always the case that the body returns to its original shape after removing the load. Solid materials flow almost like fluids at sufficiently high deviatoric stress levels (Gerstle, 2015). The plastic model is developed within the basic framework of SPLM, leaving behind the stress and strain approach.

The three essential parts of a plasticity model are

1. Yield condition (Von Mises surface),
2. Flow rule (evolution of plastic strain ϵ^p),
3. Evolution of yield surface (ignored).

3.5.1 Yield Condition

The Von Mises distortional strain energy density criterion is used by J_2 plasticity. According to this criterion, yield commences when the deviatoric strain energy density reaches a certain value. The Cauchy stress tensor is a combination of deviatoric part, $\boldsymbol{\sigma_D}$, and hydrostatic part, $\boldsymbol{\sigma_H}$, given by

$$\boldsymbol{\sigma} = \boldsymbol{\sigma_D} + \boldsymbol{\sigma_H} \tag{3.32}$$

where

$$\boldsymbol{\sigma_H} = \frac{1}{3}(\sigma_{XX} + \sigma_{YY} + \sigma_{ZZ})\boldsymbol{I}. \tag{3.33}$$

The strain tensor, ϵ, is the sum of plastic strain tensor and elastic strain tensor given by

$$\boldsymbol{\epsilon} = \boldsymbol{\epsilon^p} + \boldsymbol{\epsilon^e}. \tag{3.34}$$

J_2 plasticity is given by

$$J_2 = \frac{1}{2}\|\boldsymbol{\sigma_D}\|^2, or \tag{3.35}$$

$$J_2 = \frac{1}{6}[(\sigma_1 - \sigma_2)^2 + (\sigma_2 - \sigma_3)^2 + (\sigma_3 - \sigma_1)^2]. \tag{3.36}$$

The material yields when

$$J_2 = k^2, \tag{3.37}$$

where,
$$k = \tau_{Yield} = \frac{\sigma_{Yield}}{\sqrt{3}}. \tag{3.38}$$

Von Mises yield surface is sketched in stress space in fig. 3.4.

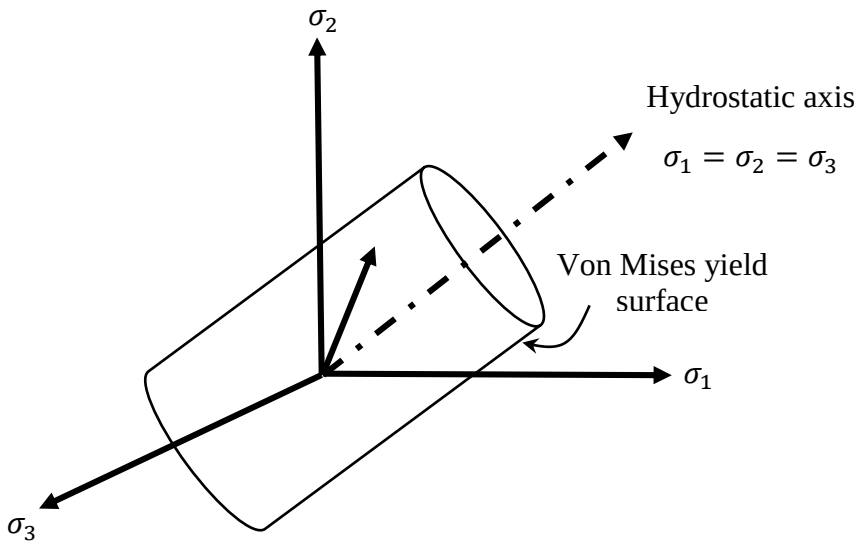

Figure 3.4 Tresca and Von Mises yield surface

3.5.2 Flow Rule

The 'Levy-Mises' flow equations are

$$d\epsilon_1^p = d\lambda\sigma_{D_1}, d\epsilon_2^p = d\lambda\sigma_{D_2}, d\epsilon_3^p = d\lambda\sigma_{D_3}, \tag{3.39}$$

where $d\lambda$ is a proportionality constant. Isochoric plastic flow is ensured because

$$d\epsilon_{volumetric}^p = d\epsilon_1^p + d\epsilon_2^p + d\epsilon_3^p = d\lambda\left(\sigma_{D_1} + \sigma_{D_2} + \sigma_{D_3}\right) = 0. \tag{3.40}$$

In terms of stress components, the flow rule can be represented as plastic strain rate versus stress

$$\begin{aligned} d\epsilon_{XY}^p &= d\lambda\sigma_{D_{XY}}, \\ d\epsilon_{YZ}^p &= d\lambda\sigma_{D_{YZ}}, \\ d\epsilon_{XZ}^p &= d\lambda\sigma_{D_{XZ}}. \end{aligned} \tag{3.41}$$

3.5.3 Evolution of the Yield Surface

Assuming perfect plasticity, we ignore this part.

3.5.4 Implementation of Plasticity in SPLM

fig. 3.5 represents briefly how plasticity is implemented in SPLM model.

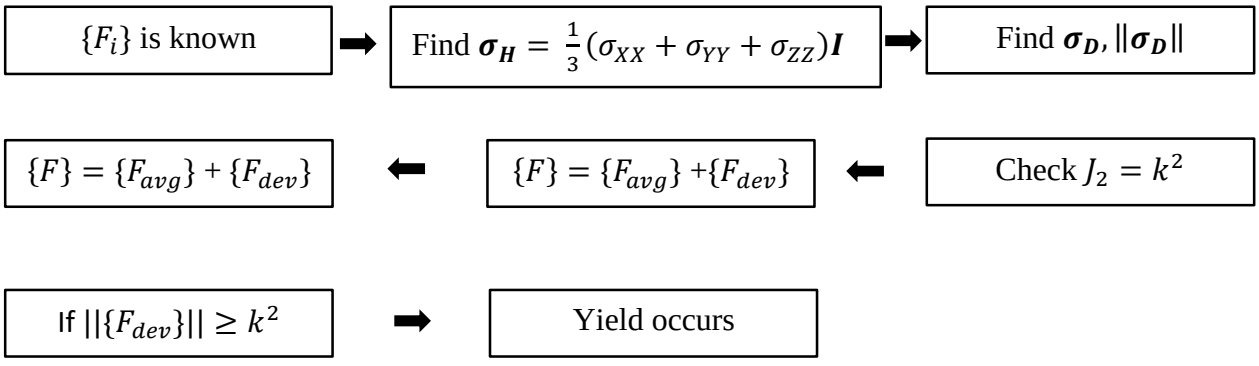

Figure 3.5 Implementation of plasticity in SPLM

If a particle yields, $\{\Delta S^p\} = \Delta\lambda\left\{\underline{F_{dev}}\right\}$. This ensures that isochoric flow occurs ($\sum \Delta S_i^p = 0$). We assume that $\Delta\lambda$ is given by

$$\Delta\lambda = \frac{\sigma_{Yield}}{E}\left(\frac{||\{F_{dev}||}{k^2} - 1\right). \tag{3.42}$$

If a particle is right on the yield surface, there will be no flow and iteration is not done within a time step. Plastic deformation does not cause a reduction in stiffness. In contrast, damage involves reduction in material stiffness with no permanent deformation upon unloading. Let us proceed to describing the damage model of SPLM.

3.6 Damage Model

Damage mechanics originated in 1958 with (Kachanov, 1958) introducing a spatially continuously-varying parameter at the macro level called the damage parameter ω. This parameter varies continuously from $\omega = 0$ to $\omega = 1$ with time. $\omega = 0$, represents no damage and $\omega = 1$, represents complete damage. Kachanov defined the uni-axial stress strain relationship as

$$\sigma = (1 - \omega)E\varepsilon, \tag{3.43}$$

where E is the Young's modulus. This relationship gives null stress when damage is complete.

We will concentrate in this chapter more on damage mechanics in the state based peridynamic lattice model, which is essential to solve problems discussed in the next chapters. The reader is encouraged to read (Gerstle, 2015) to understand more about the history of damage mechanics, the continuum damage mechanics theory and the damage mechanics for the micropolar peridynamic lattice model.

To briefly describe these models, in the continuum damage mechanics, the damage parameter at a point is assumed to depend on either the stress tensor or the strain tensor at that point. In nonlocal continuum mechanics, at a certain point, the damage is assumed to be dependent on the stress and strain which are averaged over a point's neighborhood. In the micropolar peridynamic lattice model, damage is associated with the bond and not with the particle. This may require the computational model to store more damage parameters than are necessary.

Therefore, damage model in SPLM is concerned with a single damage parameter, ω, associated with a lattice particle instead of a bond. This makes the analysis computationally simple. Less data is computed and stored because when compared to lattice particles, bonds are more in number (18 more in 3D FCC lattice models). In order for the damage to be independent of lattice rotation, it is assumed in SPLM that the damage parameter is a scalar function of the average elastic stretch in all the bonds connected to a lattice particle. A scalar damage would mean that as damage evolves, identical softening is observed in the stiffness of all the bonds connected to a particle,

$$S^e_{Avg} = \frac{1}{N_b}\sum_{j=1}^{N_b} S^e{}_j \tag{3.44}$$

$S^e{}_j$ is the elastic component of the stretch in bond i, N_b is the number of bonds connected a lattice particle. When S^e_{Avg} is greater than a critical value, damage is will initiate and evolve.

This critical value or critical average stretch is defined as

$$S^e_{AvgCritical} = \left(\frac{1-2\nu}{3}\right)\epsilon_t = \left(\frac{1-2\nu}{3}\right)\frac{\sigma_t}{E} \tag{3.45}$$

Once damage is initiated, a parameter named ‘equivalent crack opening displacement’ is introduced for the damage to evolve. This parameter is a function of the maximum total stretch of any bond S_{TotMax} that is connected to a particle. The COD equivalent is given by

$$COD_{eq} = S_{TotMax} L \tag{3.46}$$

Tensile damage evolves according to the following conditions

$$\text{if } S^e_{Avg} < S^e_{AvgCritical} \qquad \omega = \max(0, \omega_{prev}) \tag{3.47}$$

$$\text{else if } COD_{eq} \leq COD_c \qquad \omega = \max\left(1 - \frac{\gamma \frac{\sigma_t L}{E COD_{eq}} (COD_c - COD_{eq})}{COD_c}, \omega_{prev}\right) \tag{3.48}$$

$$\text{else} \qquad \omega = 1 \tag{3.49}$$

The tensile strength σ_t, the crack opening displacement COD_c, and the parameter γ define the damage model in SPLM, as shown in Fig. 3.6. This is called the elastic/cohesive SPLM damage model. After the damage initiation and evolution, further damage is dependent on the maximum elastic stretch $COD_{eq} = S^e_{Max} L$.

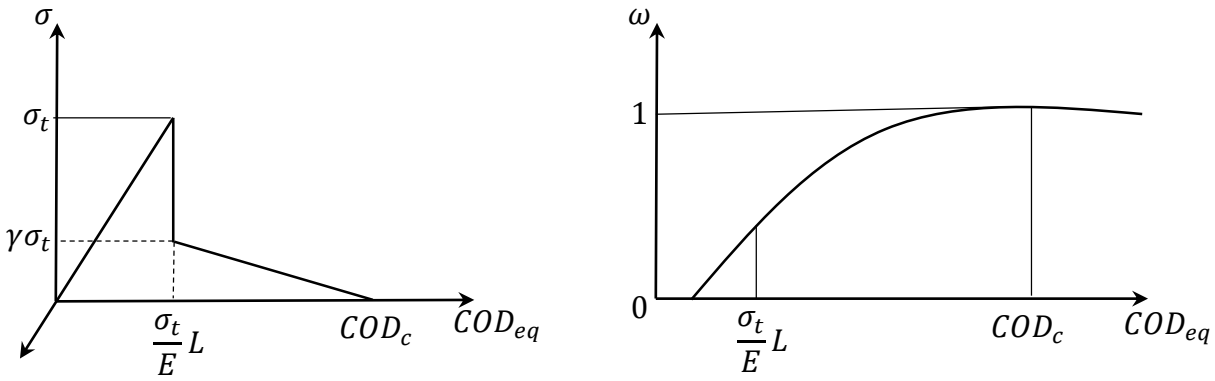

Figure 3.6 (left) $\boldsymbol{\sigma}$ versus $\boldsymbol{COD_{eq}}$ (right) $\boldsymbol{\omega}$ versus $\boldsymbol{COD_{eq}}$

Chapter 4 Concrete Uniaxial Tensile Strength

4.1 Types of Tests

The uniaxial tensile strength of concrete is determined using three methods:

1) The modulus of rupture test,
2) The direct tension test,
3) The Brazilian split cylinder test.

The direct tension test is a method to determine the tensile strength of concrete but it is a difficult test to perform. The modulus of rupture test and the Brazilian split cylinder test are both indirect tests. The modulus of rupture test, otherwise known as the flexure test, is also not frequently adopted. The Brazilian split cylinder test is a more traditional method to evaluate the tensile strength of concrete and this is because of its simplicity and convenience.

This thesis concentrates on the analysis of the Brazilian split cylinder, model the direct tension test, and the flexure test using the computational principles of the state based peridynamic lattice model. We will now describe each of the above mentioned tests adopted to measure the tensile strength of concrete.

4.2 Direct Tension Test

This method is used to determine the tensile strength of concrete by applying tensile stresses on the ends of specimens. Concrete specimens are gripping devices. In the laboratory test setup, one end of the cylinder specimen is fixed and the other end is tensioned with the gripping device. In the SPLM model of the direct tension test, we apply displacement to a layer of particles

at the top of the cylinder upwards and also apply displacement to a layer of particles at the bottom downwards. Fig. 4.1 shows the direct tension test schematically.

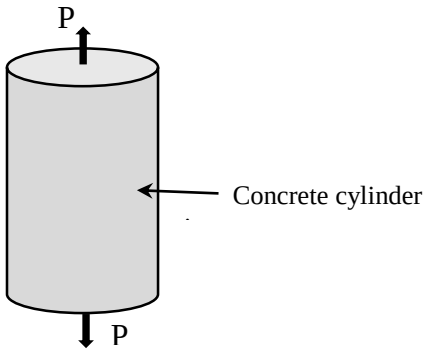

Figure 4.1 Direct Tension test

The direct tension is difficult to conduct due to secondary stresses induced at the gripping devices. The test results indicate that premature failure occurs at the ends of specimens due to stress concentration near gripping devices. The difficulty in conducting the experiment free of eccentricity also makes this test complicated (Bazant, Kazemi, Hasegawa, & Mazars, 1991). The tensile strength from direct tension test is obtained from the expression

$$\sigma_t = \frac{P}{A}, \tag{4.1}$$

where σ_t is the tensile stress, P is the peak load, A is the area of cross-section of the cylinder specimen.

4.3 Modulus of Rupture Test

The modulus of rupture test and the splitting test are indirect tests which were developed because of the difficulties experienced with the complications in direct tension test. Modulus of rupture is defined as the tensile stress assuming linear elastic conditions, at failure at the bottom face of the beam. Center point loading or symmetrical two point loading on beams is the primary method of loading used in indirect modulus of rupture test as shown in Fig. 4.2

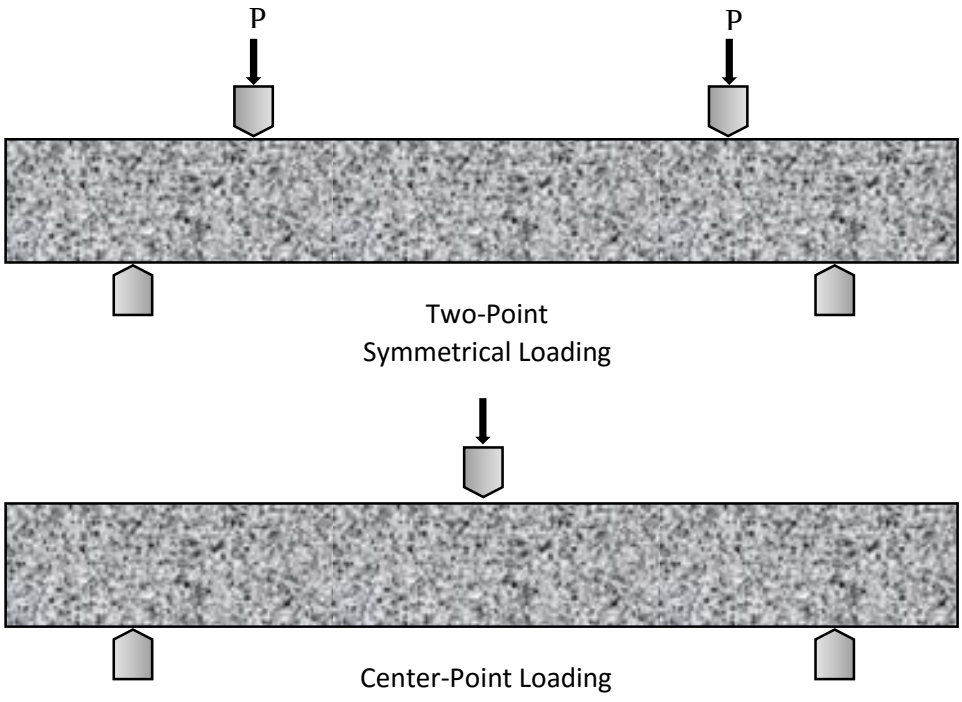

Figure 4.2 Modulus of Rupture Test

The stress obtained from the modulus of rupture test for a beam with length L, section width W, section height H, Young's modulus E and moment of inertia, I, from the classical Euler-Bernoulli beam theory is given by

$$\sigma = \frac{M.y}{I} \tag{4.2}$$

where bending moment $M = \frac{PL}{4}$ and $y = \frac{H}{2}$ in this case.

Direct proportionality of the stress with respect to the distance from neutral axis is the crucial assumption when calculating the modulus of rupture (Bazant et al., 1991). The main disadvantages of the flexure test are its sensitivity to preparation, handling, and curing of the specimen. The large weight of beam specimens often causes them to be damaged when handled and transported in the lab. Also, casting and curing of the specimens need a considerable amount of time.

4.4 Brazilian Split Cylinder Test

The split cylinder test, otherwise known as the Brazilian split cylinder test, was first introduced by Carneiro and Barcellos during the fifth conference of the Brazilian association for Standardization in 1953 (Boulekbache, Hamrat, Chemrouk, & Amziane, 2014). It has been adopted in various international concrete testing standards as a standard testing method. Some of the standards are ASTM C496, ISO 4105, and BS 1881 (Boulekbache et al., 2014).

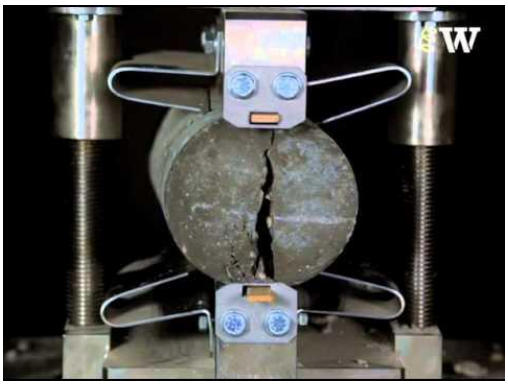

Figure 4.3 Brazilian Split Cylinder Test
(*http://www.expeditionworkshed.org*)

The Brazilian split cylinder test is an indirect measure of the uniaxial tensile strength of concrete and is considered the most reliable method (Boulekbache et al., 2014). While the direct tension test and the modulus of rupture test are not very frequently adopted due to difficulties in test methods, the Brazilian split cylinder test is a common test to determine the concrete tensile strength (Bazant et al., 1991). The split cylinder test has a simple experimental procedure and is convenient for use in the concrete laboratory since no additional equipment is needed other than what is essential for compression strength is testing.

In this test, a concrete cylinder specimen is loaded in compression diametrically using two platens (Boulekbache et al., 2014). Linear elastic theory predicts that a nearly uniform maximum principal tensile stress is produced along the diameter of the cylindrical specimen due to this

loading. This stress generated causes the cylinder to fail by splitting (Boulekbache et al., 2014). Concurrently, a compressive normal stress is also generated which is three times the tensile stress.

The split test of a cylindrical specimen produces generally a lower coefficient of variation compared to the other tests. Also, the strength obtained from the Brazilian split cylinder test is typically more than the strength obtained from the direct tension test but less than the strength obtained from flexure test (ASTM-C496/C496M 2011).

4.5 ASTM Standard Test Procedure

(ASTM-C496/C496M 2011) describes the detailed standard procedure to conduct the Brazilian split cylinder test in the laboratory. Briefly, in this test, load is applied by subjecting a concrete cylinder specimen to compression along its diameter, as show in Fig. 4.4. This specimen is placed horizontally between loading platens of testing machine. Between the platens and the specimen, strips of a soft packing material are placed. Refer to (ASTM-C496/C496M 2011) for detailed test procedure and setup.

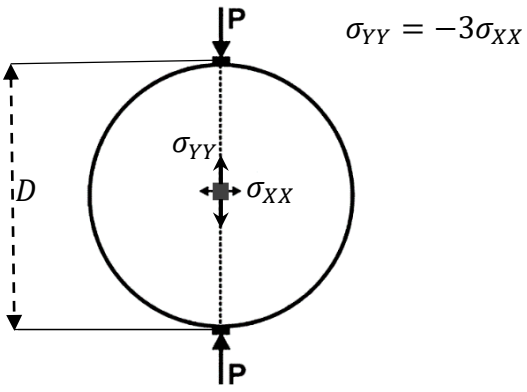

Figure 4.4 Loading setup and stresses in Brazilian split cylinder test

To estimate the tensile strength from the Brazilian split cylinder test, the classical linear elastic theory is used. The splitting strength f_{sp}, according to classical linear elastic theory is

defined as the elastic stress calculated on the basis of the tested ultimate load, P_{max} (Hoang, Andersen, Hansen, & Jónsson, 2014).

The split strength in the middle of the tested cylinder specimen is denoted as, f_{sp}. Assuming perfectly linear elastic behavior up to the point where a vertical crack through the center of the cylinder forms due to exceedance of the tensile strength, the split tensile strength of the concrete cylinder is given by

$$f_{sp} = \frac{2P_{max}}{\pi LD}. \tag{4.3}$$

P_{max} represents the maximum load obtained from the experiment. L is the thickness of the cylinder. The diameter of the cylinder is D and as mentioned before, the split tensile strength is f_{sp}.

4.6 SAP2000 Analysis

The stress distribution in a concrete cylinder under applied loads at the top and bottom nodes using the finite element software called SAP2000 is as shown in Fig. 4.5.

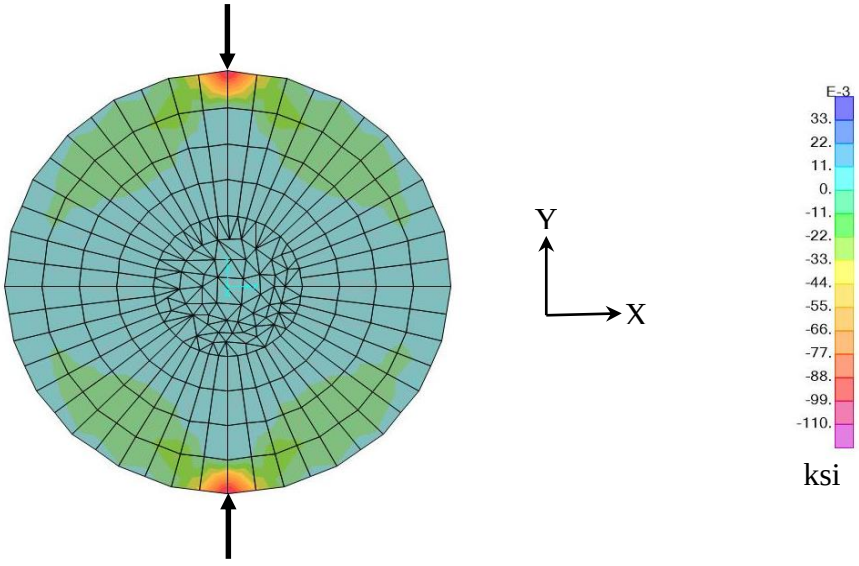

Figure 4.5 SAP2000 analysis of cylinder under compression indicating $\boldsymbol{\sigma_{XX}}$

SAP2000 is used to analyze models with linear elastic material properties. Conducting a finite element analysis of a simple 6 inch diameter cylinder with material properties of concrete helped understand how the stress concentration appeared as a result of the compressive loading. The cylinder specimen in 2D is subjected to compression under the two point loads. The σ_{XX} stress values indicated on the right in Figure 4.5 shows that the stress concentration under the loads is very high compared to the stress along the diameter.

For the given mesh, stress values can be obtained at desired locations. As the mesh is refined, this stress under the applied loads keeps increasing without limit, which is highly unrealistic. Thus linear elastic analysis is not an appropriate model for interpreting the behavior of concrete.

4.7 Comments on an Indirect Tensile Test on Concrete Cylinders (Wright, 1955)

Comments on an Indirect Tensile Test on Concrete Cylinders by Wright (1955) published in the Magazine of Concrete Research summarizes a new test that originated in Brazil to determine the tensile strength of concrete. The experimental setup of this test is such that compressive load is applied to opposite generators of a concrete cylinder specimen with strips of packing material placed between concrete cylinder specimen and loading platens. This method involves applying a compressive load to a cylinder which sets up a nearly uniform tensile stress over the plane along the diameter of the cylinder. The specimen then fails in tension across the diametral plane of loading.

In the paper, the study conducted investigates the effect of packing strip material and dimensions on the strength. A comparison of results from the Brazilian test, the direct tension test and the modulus of rupture test is made.

The effect of size of specimen on the strength is also analyzed. The specimen sizes for each of these tests are shown in Table 4.1 and Fig. 4.6.

Table 4.1 Dimensions of test specimens

TEST	CONCRETE SPECIMEN SIZE
Brazilian split cylinder test	D = 6 inch, L = 12 inch
Direct tension test	D = 4 inch, L = 18 inch
Modulus of rupture test	W = 4 inch, H = 4 inch, L = 12 inch

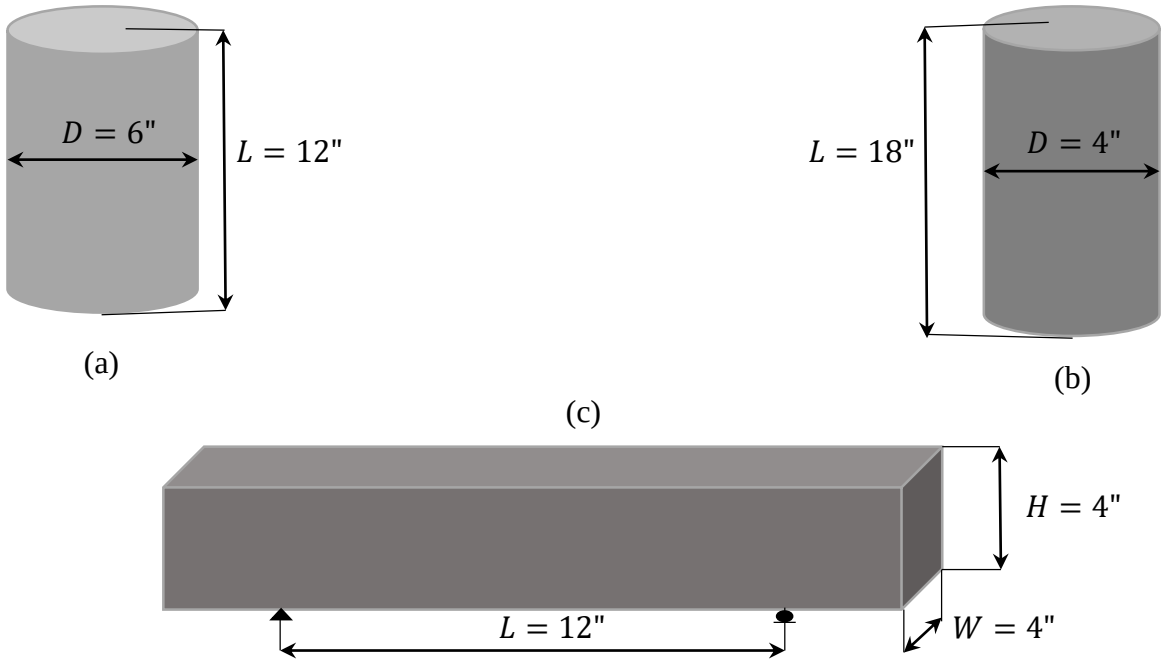

Figure 4.6 Specimen sizes for (a) Brazilian split cylinder test (b) Direct tension test

(c) Modulus of rupture test

Our interest lies in comparing the results from these tests to the results obtained from SPLM simulations of these tests. The compressive strength of concrete was obtained to be 5980 psi. We will use this f_c in our SPLM models. The average value of tensile strength obtained by testing 32 specimens of each type are shown in Table 4.2.

Table 4.2 Concrete properties

Type of Test	**Average Strength (lb./sq.in.)**
Brazilian split cylinder test	405
Direct Tension Test	275
Modulus of rupture of beams	605

We use the tensile strength F_t obtained from the direct tension test as the tensile strength of concrete in the SPLM models. We will back calculate the peak load from each of the laboratory test results using Equations 4.1, 4.2, and 4.3. These peak loads can be later compared to the peak loads obtained from the SPLM simulations.

1) Brazilian split cylinder test

$$P_{split} = \frac{\pi L D f_{sp}}{2} = \frac{\pi * 12\ inch * 6\ inch * 405\ psi}{2} = 45.8\ Ki \tag{4.4}$$

2) Direct tension test

$$P_{direct\ pull} = F_t \times \frac{\pi D^2}{4} = 275\ psi \times \frac{\pi \times (4\ inch)^2}{4} = 3.45\ kip \tag{4.5}$$

3) Modulus of rupture test

$$P_{rupture} = \frac{4\sigma I}{Ly} = \frac{4 \times 605\ psi \times (\frac{4^4}{12})}{12 \times (\frac{4}{2})} = 2.15\ kip \tag{4.6}$$

In Chapter 5, we study the objectivity of SPLM by modelling the Brazilian split cylinder test. We will see the time dependent analysis, effect of the position of loading plate on the bonds between steel and concrete, and the interaction of steel and concrete lattice bodies.

Chapter 5 Investigation of the Objectivity of SPLM

The primary purpose of this chapter is to understand the objectivity of the state based peridynamic lattice model and analyze the behavior of plain concrete. In this chapter, a time dependent analysis is conducted. We will address three main aspects in this objective study:

1. Firstly, the effect of change in the loading rate on the peak load and crushing patterns of the plain concrete split cylinder specimen is studied. From the analysis, we will obtain the time of simulation time needed to get reasonable test results. It is very important to understand how long the displacement must be applied because peridynamic study is a non-linear time dependent analysis. We can also understand with this test the computational power needed to solve simple problems and obtain solutions.
2. The second aspect we will study is the loading condition of the Brazilian split cylinder. The position of the steel platens, to which displacement is applied, is changed and the results are observed. The interaction between steel and concrete lattice bodies can be further understood with these tests. The position of the steel platen which gives reasonable results is considered. The plasticity and damage models of plain concrete can be further understood from this analysis.
3. The next important aspect is the effect of lattice rotation on the concrete specimens. We will rotate the lattice and observe the percentage difference in the results in Chapter 6.

5.1 Specifications for the Brazilian Split Cylinder Test

To perform a nonlinear analysis of the Brazilian split cylinder test, a 6 inch diameter cylinder with a thickness of 12 inch is loaded in compression along its diameter as shown in Fig. 5.1.. The smooth time-varying displacement-controlled loading is given by $\Delta_Y(t) = \frac{\Delta_{max}}{2}\left(1 - \cos\left(\frac{\pi t}{t_{end}}\right)\right)$, as shown in Fig. 5.2.

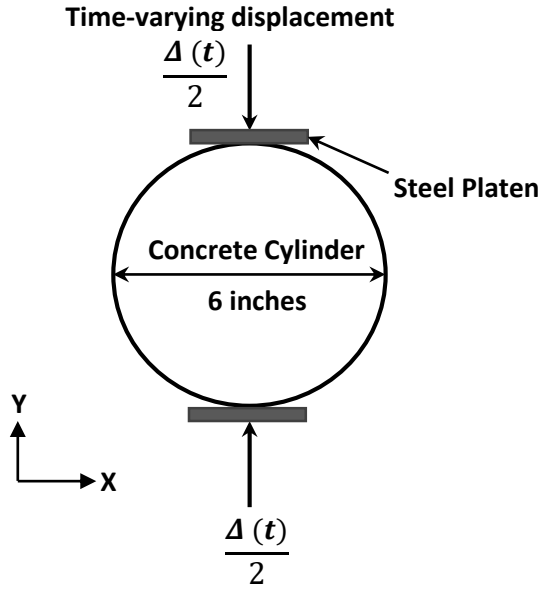

Figure 5.1 Brazilian split cylinder

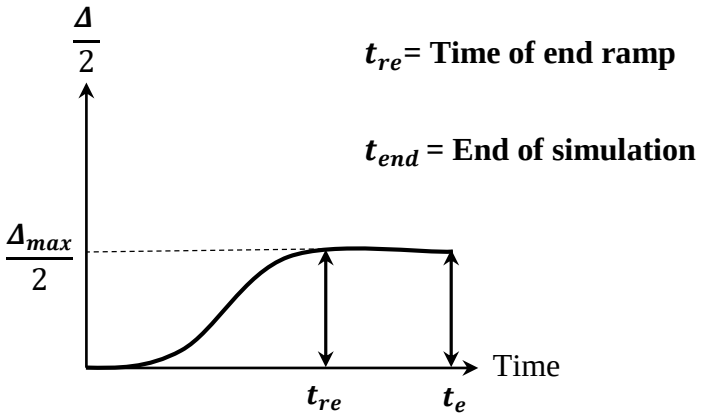

Figure 5.2 Time varying displacement

A uniaxial compressive strength of f'_c = 5980 PSI for a normal strength concrete is used for this problem which is obtained from the laboratory according to (Wright, 1955). Lattice spacing for both lattice bodies, steel and concrete, is considered to be a constant value of 1 cm. This is a lower limit value beyond which the normal concrete is certainly no longer homogeneous (Gerstle, 2015). For two-dimensional problems, a hexagonal lattice is used. The material parameters are given in Table 5.1.

Table 5.1 Material properties of concrete

Parameter	**English Value**	**SI Value**
Compressive Strength, $F'_c = \sigma_{\text{yield}}$	5980 PSI	41.23 MPa
Young's modulus, E	3605 KSI	30.39 GPa
Poisson's ratio, ν	0.20	0.20
Lattice spacing, L	0.3937 inch	1.0 cm
Internal damping ratio, ζ_{internal}	0.2	0.2
Uniaxial tensile strength, $F_t = \sigma_t$	400 PSI	1.896 MPa
Ultimate tensile damage crack opening displacement, w_c	0.008736 inch	0.2 mm
Tensile damage parameter gamma, γ	0.25	0.25
Fracture energy G_F	0.787 lb./inch	137.9 N/m

For the SPLM analysis, the fundamental period of a concrete cylinder is to be obtained. The fundamental period of a structure is estimated by analyzing it as an elastic problem. This can

be done using SAP 2000, which is a linear elastic code. For a cylinder with dimensions mentioned above and with both bottom and top nodes pinned, the fundamental period ($T_{fundamental}$) was found to be 0.00025 seconds.

The critical time step required for a linear elastic dynamical simulation is calculated based on the lattice spacing, damping ratio and the speed of sound. The critical time step Δt is 3 x 10^{-7} seconds. To efficaciously simulate the quasistatic loading of the Brazilian split cylinder using the SPLM, an approximately accurate value for time of simulation must be obtained which is given by $n \times T_{fundamental}$. After obtaining this value, the number of time steps is then given by

$$t_{endTimeStep} = \frac{n \times T_{fundament}}{\Delta t} \tag{5.1}$$

The computational model of the concrete cylinder must faithfully simulate both the behavior of concrete and the steel platen. The bond between concrete and steel should be interpreted accurately. Plain concrete is modeled using the elasticity, plasticity and damage models discussed earlier.

5.2 Steel Platens

The steel platens, both on top and bottom, have a width of 4 cm and a thickness of 2 cm. The stiffness of the steel platen takes into account the plywood strip used in the laboratory. Thus the stiffness of the steel platen is lower than the actual steel stiffness. The position of the steel platen requires to interact with the concrete particles in a stabilized manner is needed. Lattice spacing in both the material bodies is assumed to be same. The force in an individual SPLM bond between steel and concrete lattice particles with stretch S is given by

$$F = (1 - \omega_{concrete}) a_{concrete} \left(\frac{m_{steel}}{m_{concrete}} \right) S. \tag{5.2}$$

Here, $a_{concrete}$ is the stiffness parameter for the concrete body, $\frac{m_{steel}}{m_{concrete}}$ is a factor which ensures that the elastic stiffness of the bonds between steel and concrete are not so high that numerical instability arises. In all the simulations, to make certain that the loading plates are simulated as perfectly elastic, both the damage flag and plasticity flag for the platen are turned off. The SPLM parameters of steel loading plates are given in Table 5.2.

Table 5.2 Steel loading plates - Material parameters

Parameter	**English Value**	**SI value**
Yield Strength, $F_Y = \sigma_{yield}$	60,000 PSI	413.7 MPa
Young's modulus, E	29,000 KSI	200.0 GPa
Poisson's ratio, ν	0.30	0.30
Mass Density, ρ	490 PSF	7849. Kg/m^3
Lattice spacing, L	0.3937 inch	1.0 cm
Support size in Y	1.5748 inch	4.0 cm
Damping Ratio, ζ	0.2	0.2

5.3 Time Dependent Analysis

The SPLM simulation is conducted under quasistatic loading conditions. For this, the modeler must approximate the fundamental period of the structure and then consider the suitable time of simulation which is a function of this period. But what value of this time of simulation gives reasonable results? To answer this, SPLM simulations with six multiples of the fundamental period are conducted. The SPLM model of concrete cylinder at the beginning of loading is shown in Fig. 5.3.

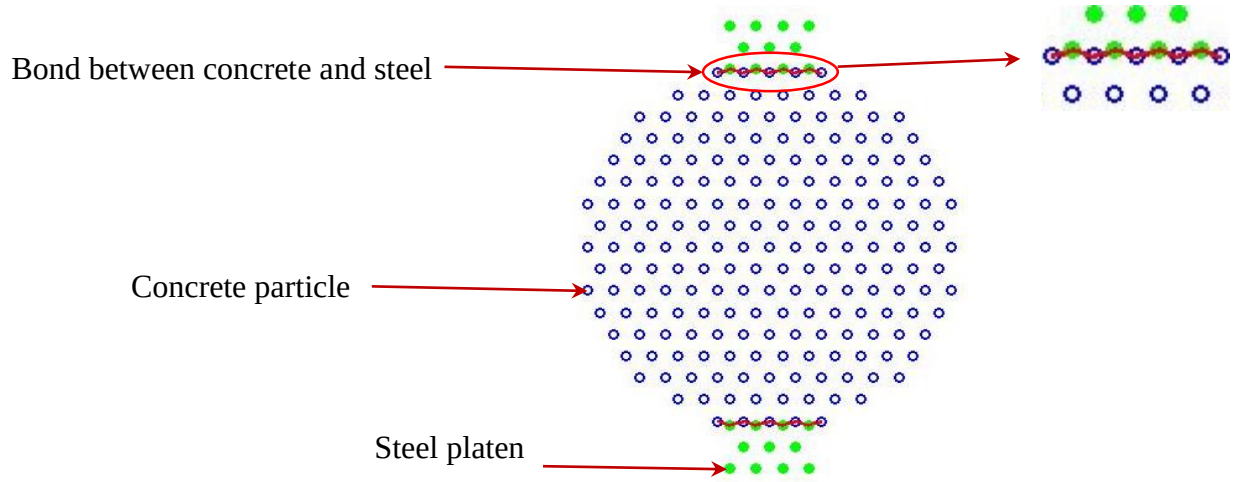

Figure 5.3 Initial SPLM model for $\mathbf{2 \times T_{fundamental}}$

Consider the first case with time of simulation of $2 \times T_{fundamental}$. This indicates a reasonably fast rate of loading and thus represents a dynamic load application. The concrete lattice is represented by the blue colored particles. The green particles represent the steel loading platens. The red lines indicate the external links or the bonds between steel and concrete.

With a significant amount of concrete crushing and damage, the peak load was 790 kN when analyzed for $2 \times T_{fundamental}$. After analyzing for a longer time duration, we will be able to decide which value can result in reasonable values of peak load and concrete behavior. Similar analysis is conducted for different time of simulation and the results are observed. The final stage of loading for $2 \times T_{fundamental}$ is shown in Fig. 5.4.

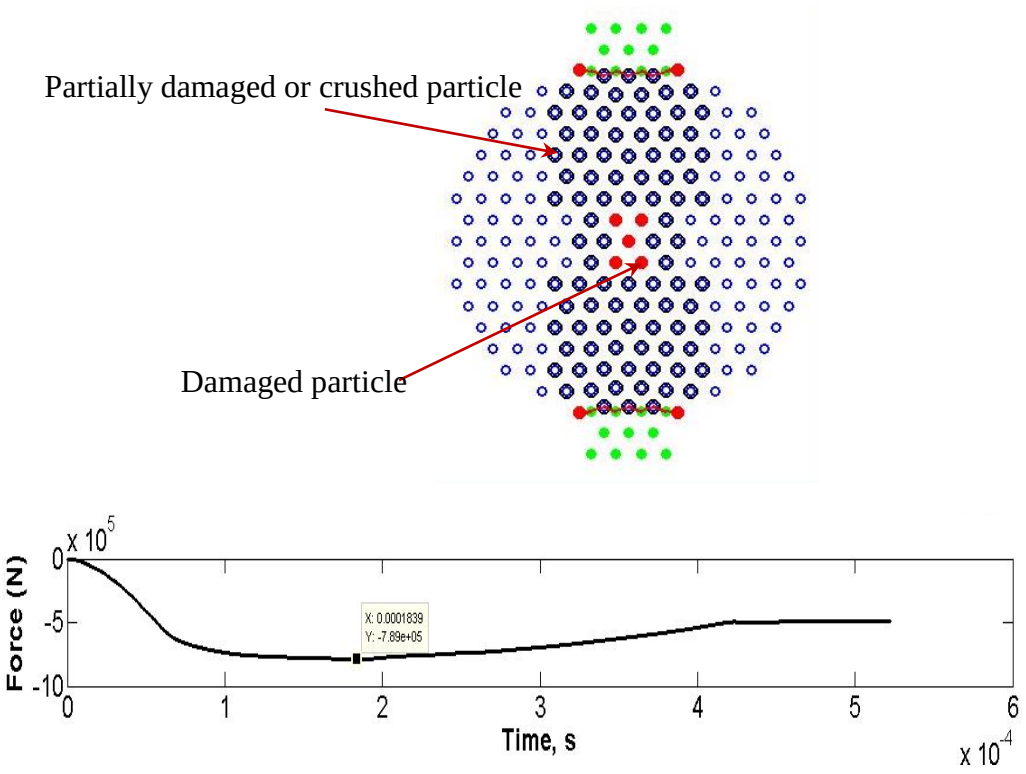

Figure 5.4 (top) Final SPLM model (bottom) Force vs Time

The large difference between the residual and the peak values of load indicates that the displacement is being applied suddenly to the steel platens. Instead of simulating a gradual load application in this case, the SPLM simulates a sudden or dynamic load. This is not the desired loading method to obtain reasonable results.

It can be noted that along the diameter, concrete crushes and under the load, there is compressive plastification. This means that concrete is failing under the compressive loads diametrically. Further analysis is conducted with 4, 8, 16, 32, 64 and 128 times the fundamental period. The final SPLM models are shown in Fig. 5.5.

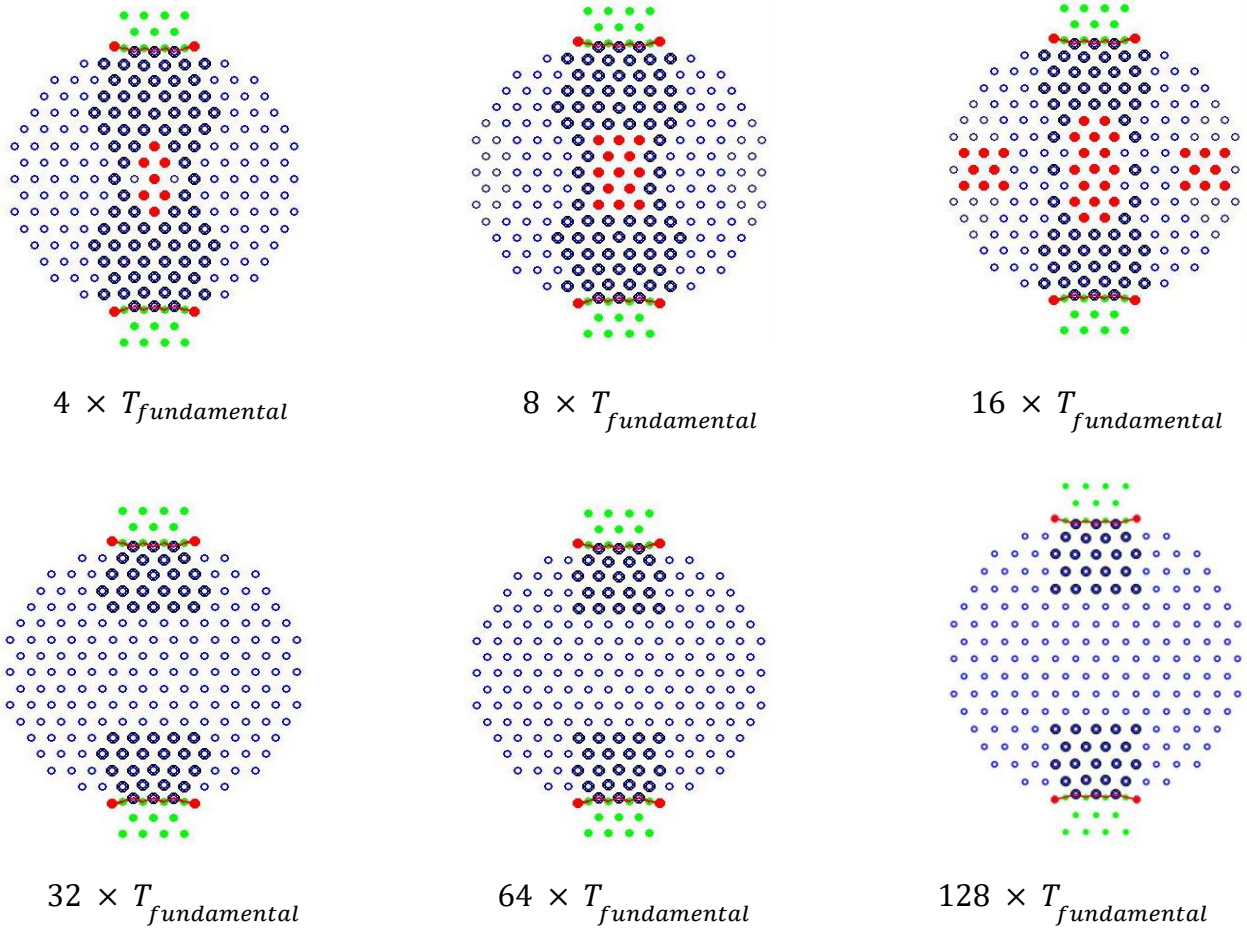

Figure 5.5 SPLM models for six different simulation time

It was observed that as the time of simulation increases, the peak and the residual loads come closer. Also, the concrete behavior changes from one simulation to the other. The peak and residual loads are observed to be much closer when the analysis is conducted for greater *n* values. From *n* = 16 to 128, the maximum and residual loads vary within 1% - 3%.

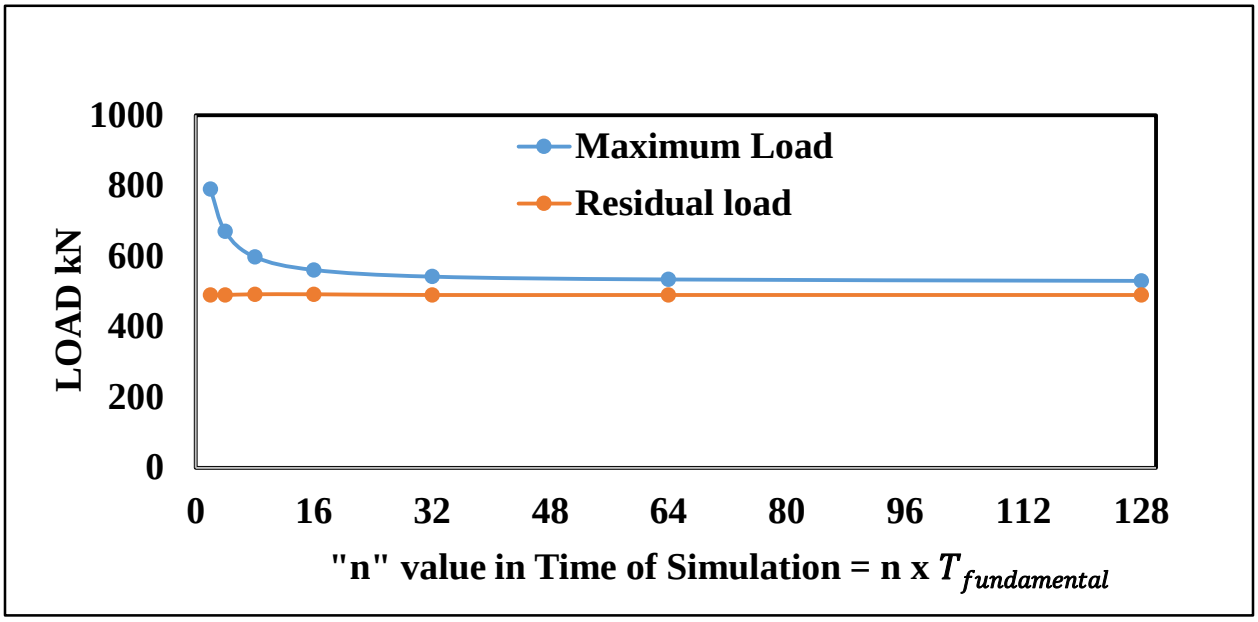

Figure 5.6 Plot of Load vs n

It can be concluded from this analysis that in order to obtain a reasonable results within a 2% difference between peak loads from the quasistatic loading condition in SPLM, it is advisable to conduct the analysis for a time of simulation of *16* x $T_{fundamental}$. If the user demands more accuracy, then it is advisable to perform the analysis for a longer time of *128* x $T_{fundamental}$ keeping the computational power in mind.

5.4 Position of Plate on Bond, Crushing and Peak Load

To understand the changes in orientation of bond and subsequently the loading condition, the steel platen position must be analyzed. The center of the steel support is shifted from one point to another vertically as a function of the diameter of the cylinder specimen (D), support size (S) and the lattice spacing (L). To review the parameters used for this problem, see Table 5.1 and Table 5.2.

The top of the cylinder is at diameter/2 which is 0.075m from center (O). Consider the center of the steel platen (C) from the top of specimen within +0.01m range and -0.01m range from bottom of the cylinder as shown in Fig 5.7.

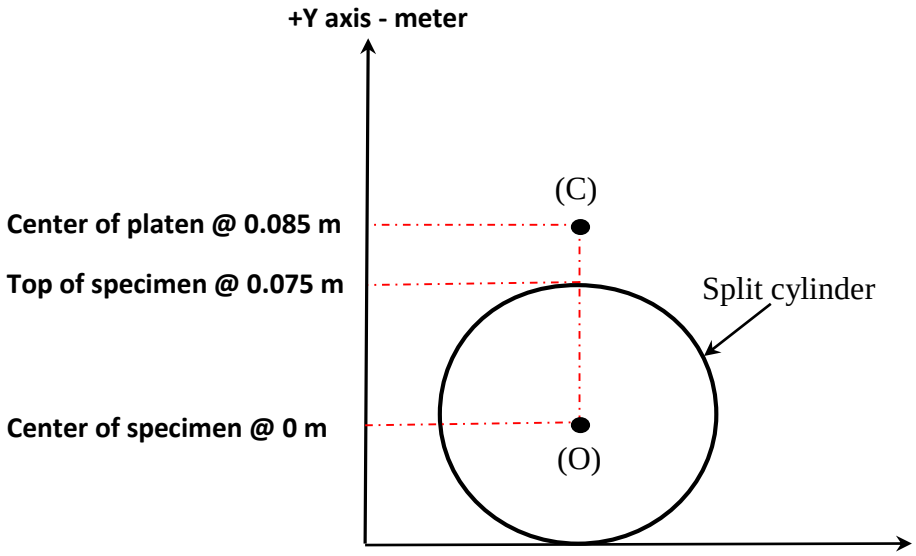

Figure 5.7 Schematic depecting the points of interest

SPLM analysis is conducted with various plate positions as shown in Fig 5.8, and the resulting interaction between concrete and steel is studied. That position of the plate which gives an adequate overlap in the reference configuration between steel and concrete lattice bodies in order to ensure stability between the two bodies is obtained from these tests.

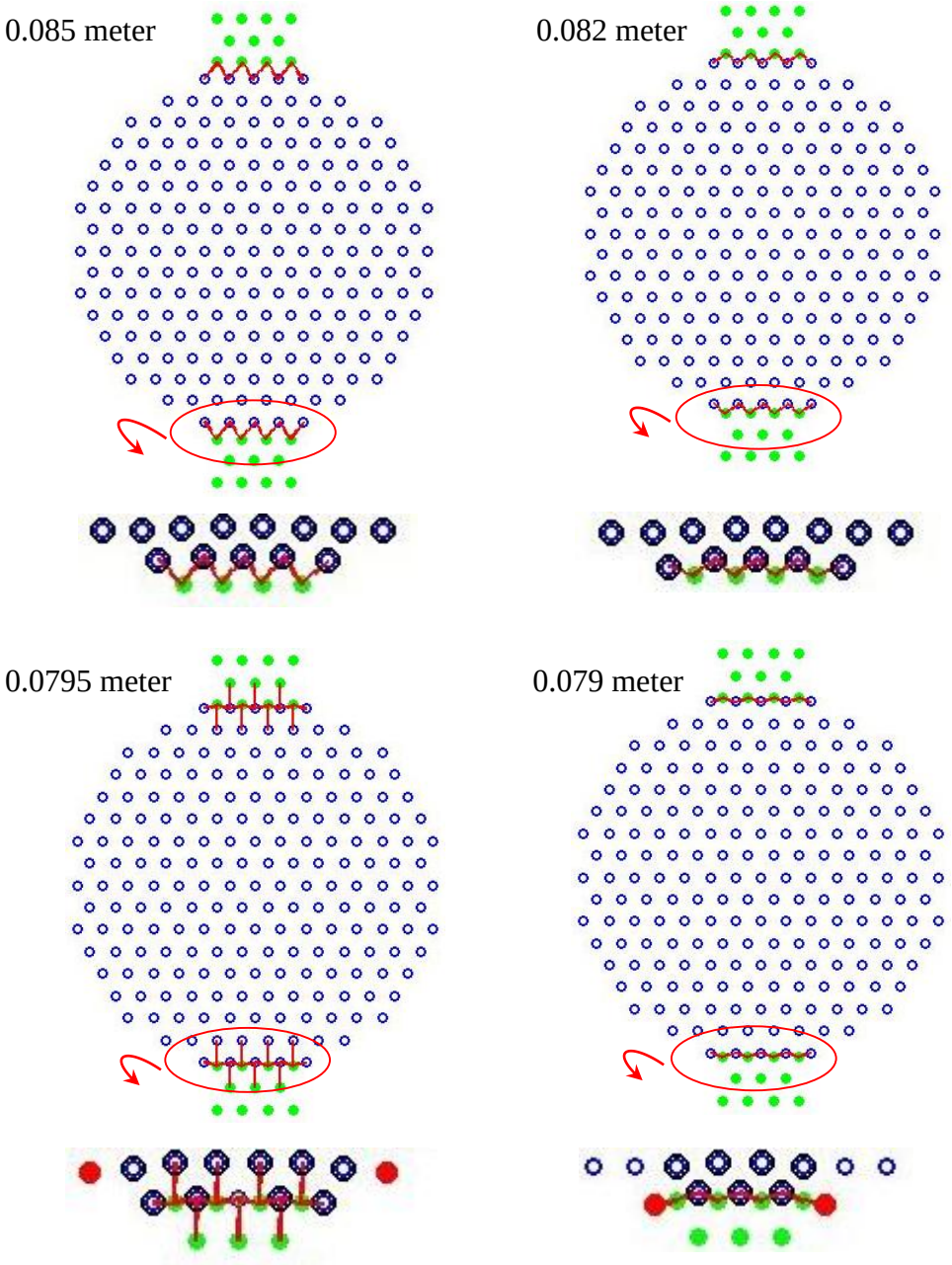

Figure 5.8 SPLM model indicating orientation of bonds for different cases

The bond configuration between steel and concrete changes from when the center of the top plate is at 0.085 m to 0.082 m from the center of the cylinder. When the center of the top platen

moves closer and closer to the top of the split cylinder, the angle that the bond makes with the horizontal reduces even more until it becomes 90 degrees at 0.0795 m. In this case, the bond becomes perpendicular to the horizontal and the orientation can be clearly observed.

One interesting observation is that when the center of the top platen is shifted from 0.0795 m to 0.079 m from the center of the cylinder, the interaction between the steel and the concrete particles is behaving very different compared to the other cases. The bond between these two materials seems to be 'snapping' through creating an instability issue. This is the plate position we would want to avoid in our simulation. The plot between the positions of the center of the top plate from the center of the cylinder in meters on Y axis versus the load in kilo Newton on X axis is in Fig. 5.9.

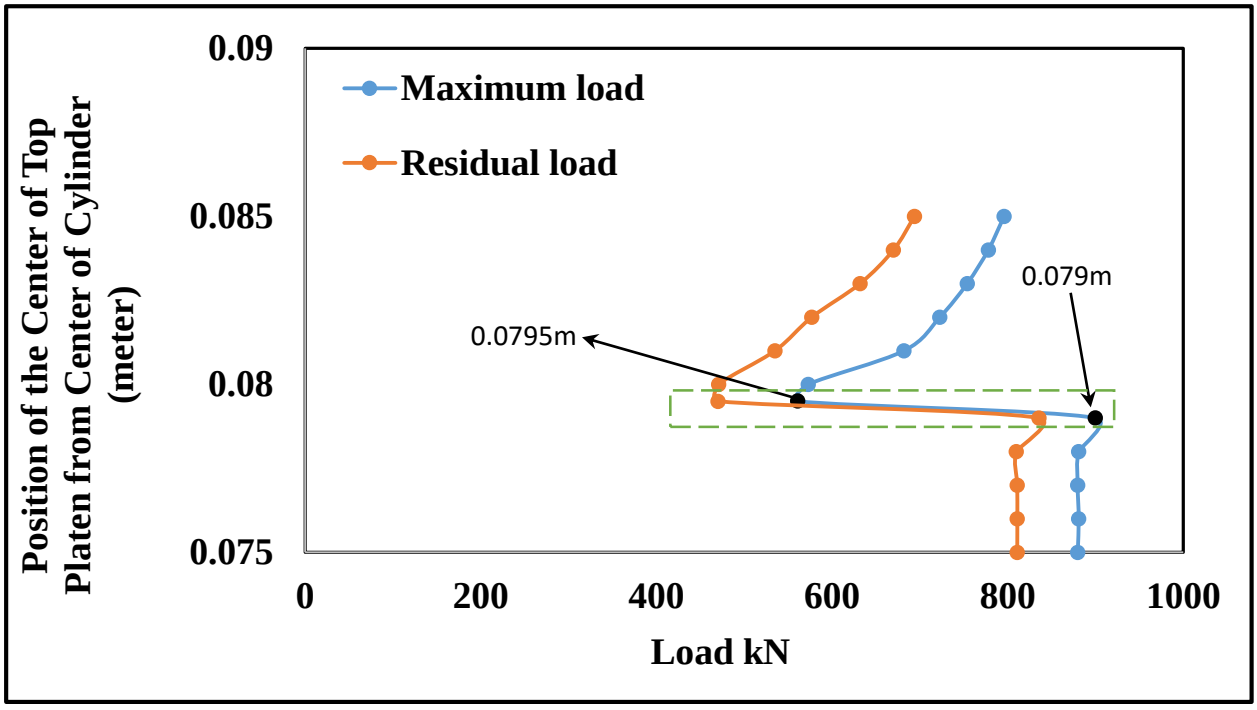

Figure 5.9 Plot of position of "center of top steel platen" vs "Load"

The transition highlighted indicates that when the center of the top platen is shifted from 0.0795 m to 0.079 m from the center of the cylinder, the change in peak loads between the two positions is very large. This position of the plate which gives an instable interaction between steel and concrete particles needs to be avoided in the SPLM simulation of the Brazilian split cylinder test in order to get reasonable results. It should also be noted that for stable interactions between steel and concrete lattice bodies, the position of steel platen has a significant change of around 7% on an average in the peak load values. An aspect to think about here is whether the Brazilian split cylinder test is reasonable when the values of peak loads from the test are affected interaction with the loading platen.

5.5 Bond Configuration

Consider a nonlinear elastic analysis of the split cylinder with the position of top and bottom plate at 0.0795 m from the center of the cylinder. A non-linear elastic analysis can be achieved by turning off the plasticity and damage models and simulating only the elastic model in the pdQ. The nonlinear analysis of the split cylinder can help us understand better how the bonds between steel and concrete work and if there is any issue which must be understood for the sudden drop in loads. For this, let us observe the variation of load with time. Figure 5.10 shows SPLM simulation of the Brazilian split cylinder test at three different stages of time.

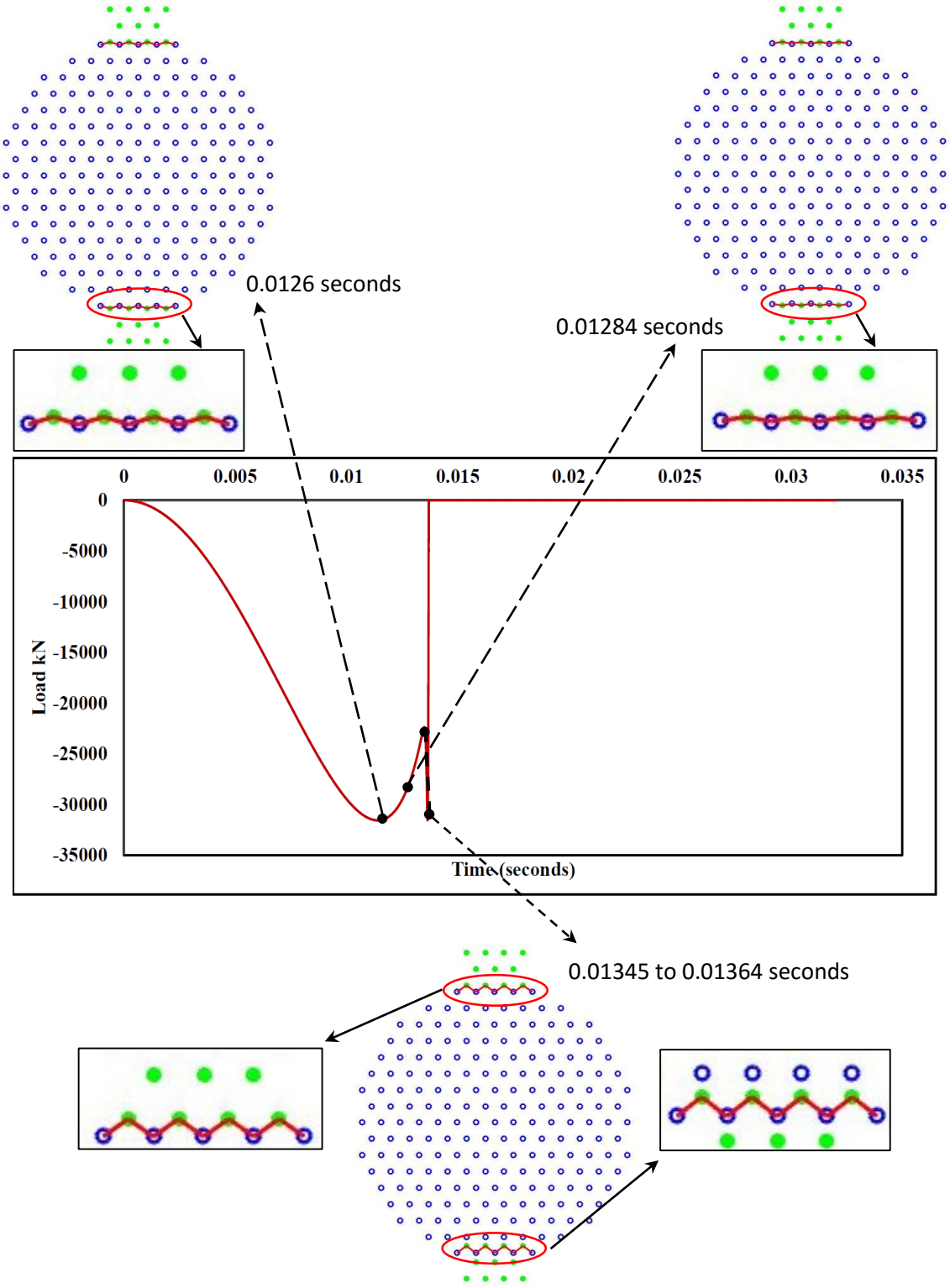

Figure 5.10 Different stages in split cylinder simulation

The orientation of bonds between steel and concrete lattice bodies transitions gradually for a certain time. The load increases to a certain value and then starts decreasing gradually down to a point. After this point of time, there is a sudden decrease in load and the bonds between steel and concrete in this phase snap through. This would be the phase where the bonds are acting in an instable manner. After this phase, the load drops down to 0 kN and remains 0 kN until the completion of the analysis. The time phases in which this behavior is observed can be clearly noted in Figure 5.10.

Let us eliminate the plate for now and observe how the load varies when displacement is applied to the concrete particles of the lattice instead of a steel loading platen. The top and bottom particles of the concrete split cylinder are subjected to a time-varying displacements. In other words, the cylinder is subjected to compression without interaction of concrete with any other material. The SPLM model without plate is shown in Fig. 5.11.

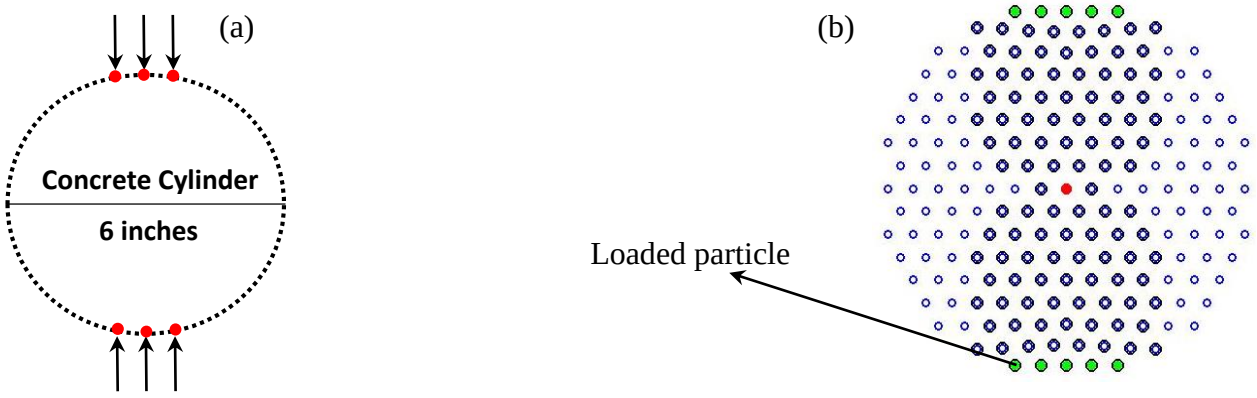

Figure 5.11 Split cylinder without steel plate (a) Schematic and (b) SPLM model

This clearly indicates concrete plastification under direct application of load to the particles. Conducting a time dependent analysis indicates that the peak loads are within 5% difference for the different simulation time similar to what was observed for the split cylinder with steel platen. Therefore, the analysis can be conducted for $16 \times T_{fundamental}$, as indicated by Fig. 5.12.

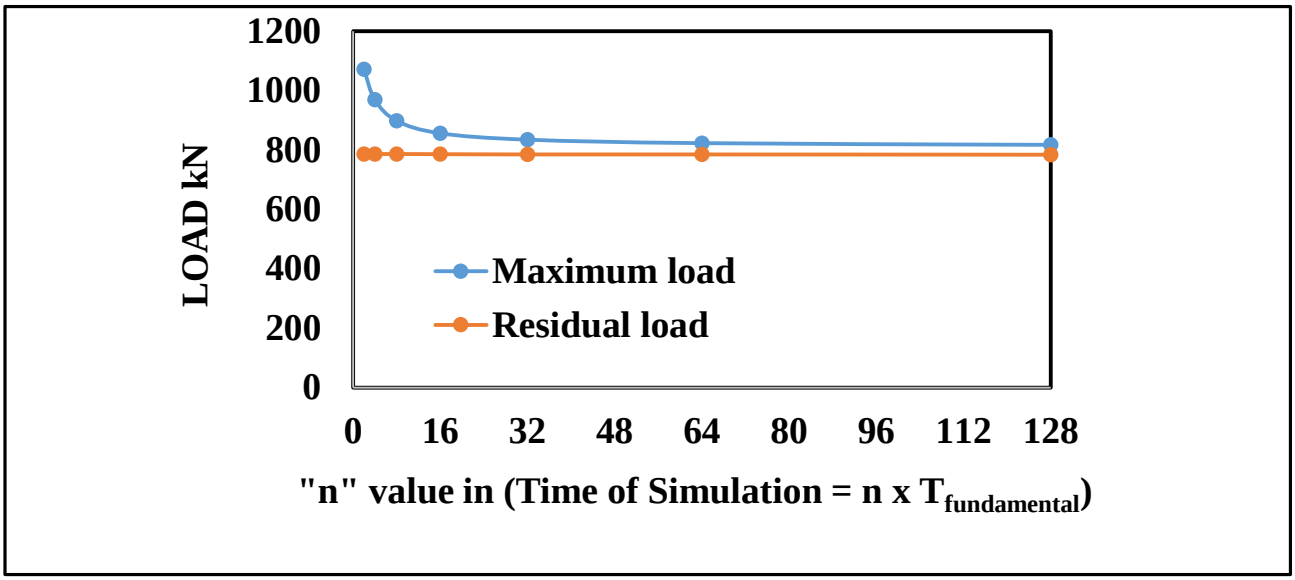

Figure 5.12 Plot of Load vs n

Now, with adequate information regarding the position of the steel loading platen, a stable concrete-steel interaction condition and a reasonable time of simulation, we proceed to modelling the Brazilian split cylinder test, the direct tension test and the modulus of rupture test. The peak loads obtained from the SPLM simulations are then compared to the peak loads obtained from the laboratory tests conducted in (Wright, 1955).

Chapter 6 SPLM Analysis of Lab Specimens

6.1 Brazilian Split Cylinder Test

The peak load obtained from (Wright, 1955) for the Brazilian split cylinder test is $P_{lab} = 45.8\ kip$. The peak load obtained from SPLM analysis for $\theta = 0^0$ is $P_{SPLM} = 126\ kip$. The plots between displacement, time and force for the split cylinder simulation are shown in Fig. 6.1.

Therefore,
$$\frac{P_{SPLM}}{P_{Lab}} = \frac{126\ kip}{45.8\ kip} = 2.75. \tag{6.1}$$

(a)

(b)

(c)

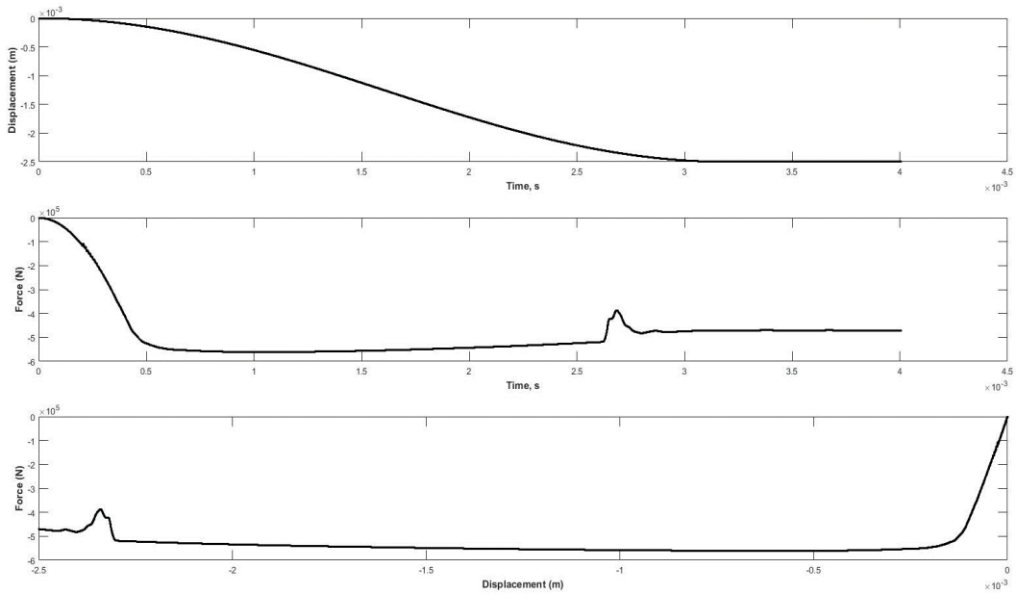

Figure 6.1 (a) Displacement vs. time (b) Force vs. time (c) Force vs. displacement for Brazilian split cylinder test at $\boldsymbol{\theta = 0^0}$

We now simulate the concrete cylinder rotated 0^0 and 30^0 counterclockwise. Applying the same displacement to the steel loading platens, the plastification and subsequent tensile cracking pattern is observed in all the three cases.

It can be seen that there is a slight variation in the damage and fracture behaviour with change in lattice rotation. The peak load observes a 17% increase when transitioning from a lattice with $\theta = 0^0$ to a lattice with $\theta = 30^0$. These errors are imputed to variations in modelling the exact dimensions when lattice is rotated. It is however clear that the damage and plasticity models in SPLM behave as expected. The damage patterns for models with different lattice rotations are shown in Fig. 6.2.

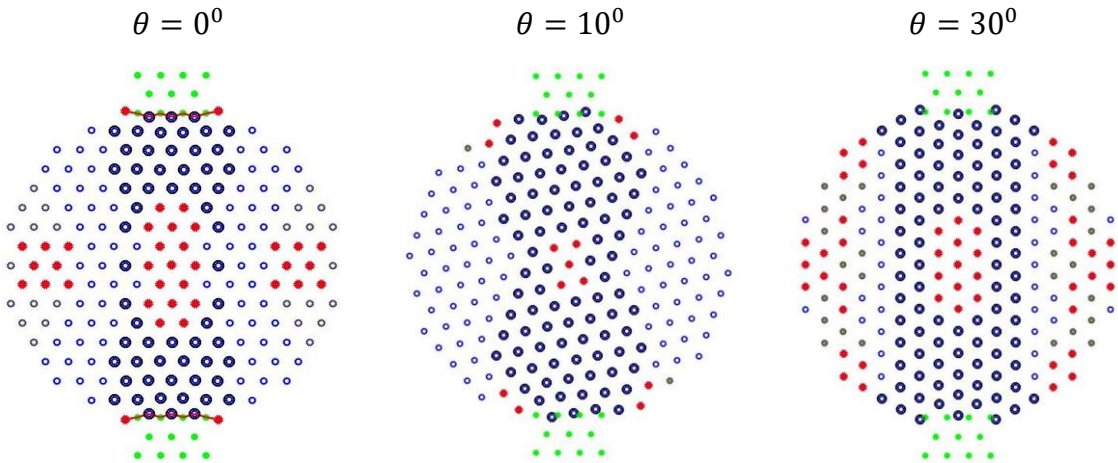

Figure 6.2 Damage patterns as a function of lattice rotation for Brazilian split cylinder

6.2 Direct Tension Test

For the tension specimen, the fundamental period from SAP2000 was obtained to be 0.00019 seconds. For this test in SPLM, the top and bottom two layers of particles were subjected to a time-varying displacement. Peak load obtained from (Wright, 1955) for the direct tension test is $P_{lab} = 3.45\ kip$. Peak load obtained from SPLM analysis for $\theta = 0^0$ is $P_{SPLM} = 3.72\ kip$. The plots between displacement, time and force for the split cylinder simulation are shown in Fig. 6.3.

Therefore,

$$\frac{P_{SPLM}}{P_{Lab}} = \frac{3.72\ kip}{3.45\ kip} = 1.07 \tag{6.2}$$

(a)

(b)

(c)

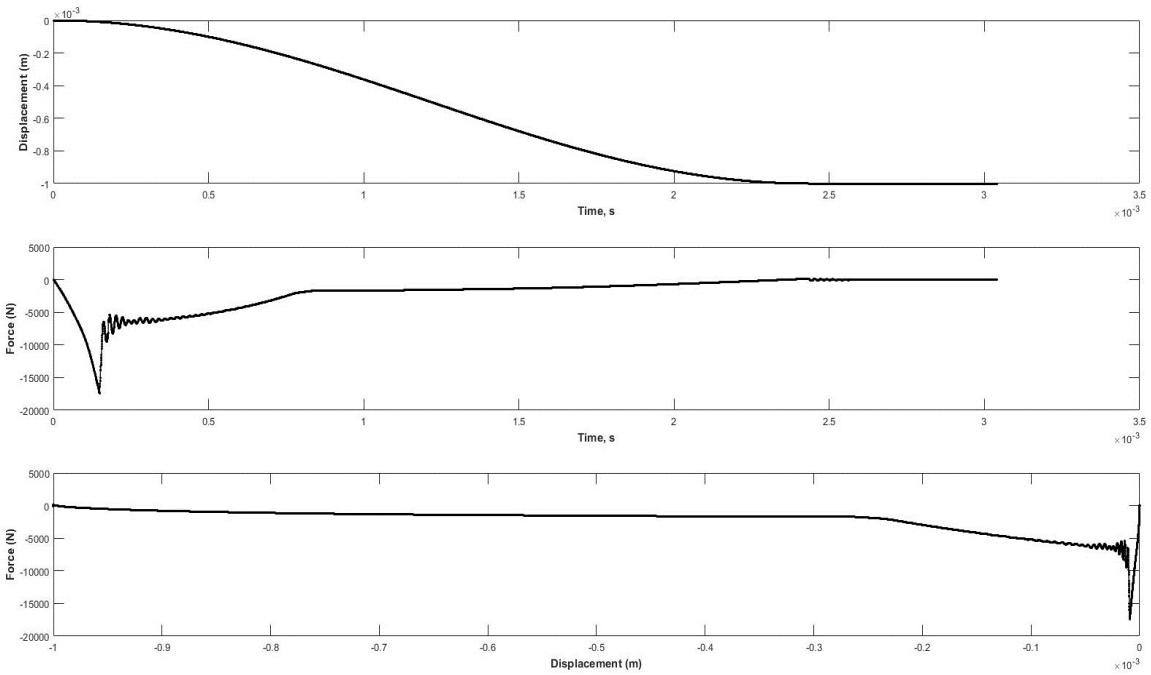

Figure 6.3 (a) Displacement vs. time (b) Force vs. time (c) Force vs. displacement for direct tension test

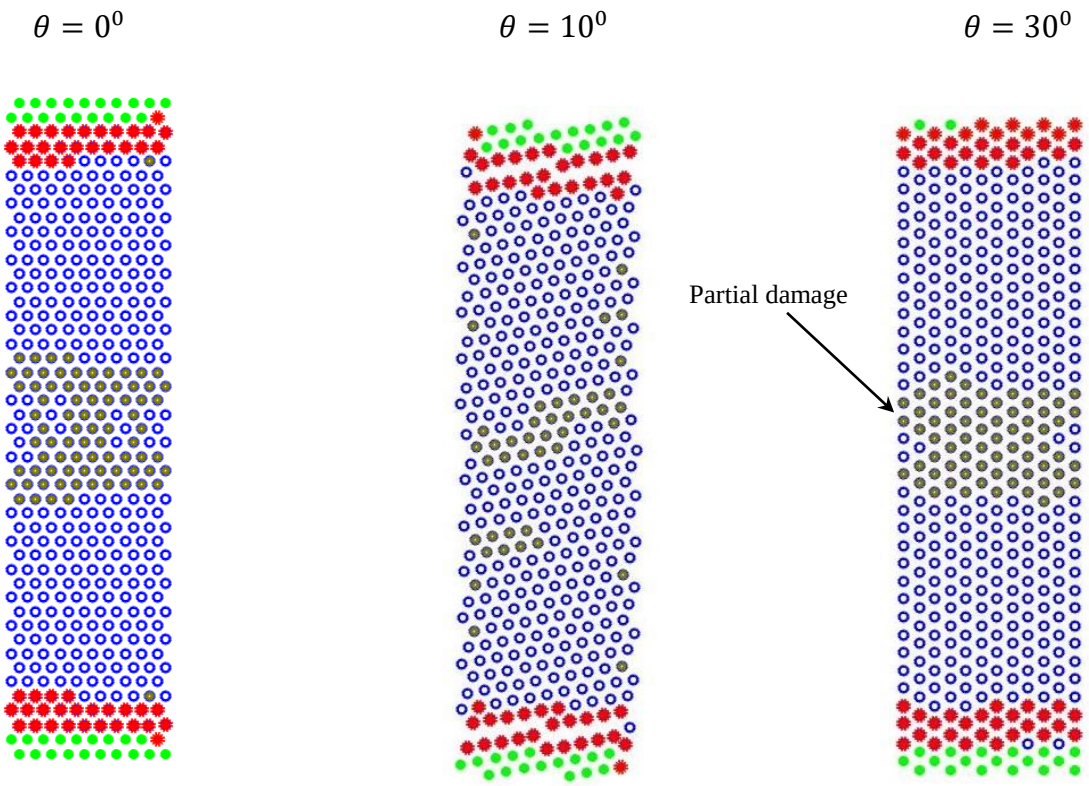

Figure 6.4 Damage patterns as a function of lattice rotation for direct tension test

Similar analysis of rotation of concrete lattice with the tension specimens in direct tension test is conducted. The crushing patterns in the three concrete specimens with lattice rotation angle of $\theta = 0^0, 10^0, 30^0$ respectively can be seen in Figure 6.4.

The difference in peak load at $\theta = 0^0$ and $\theta = 30^0$ is 17%. Though there is a slight variation in the damage and fracture behavior, as well as the values of peak load, the reason is clearly understood as discussed earlier.

6.3 Modulus of Rupture Test

For the flexure beam, the fundamental period from SAP2000 was obtained as 0.0005 seconds. Three top particles in the center of the beam were subjected to a time-varying displacement. The displacement applied to these particles was calculated from the deflection equation $\Delta = \frac{PL^3}{48EI}$. Peak load obtained from (Wright, 1955) for the modulous of rupture test is $P_{lab} = 2.15\ kip$. Peak load obtained from SPLM analysis for $\theta = 0^0$ is $P_{SPLM} = 4.07\ \ kip$. The plots between displacement, time and force for the split cylinder simulation are shown in Fig. 6.5.

Therefore,

$$\frac{P_{SPLM}}{P_{Lab}} = \frac{4.07\ kip}{2.15\ \ kip} = 1.9 \tag{6.3}$$

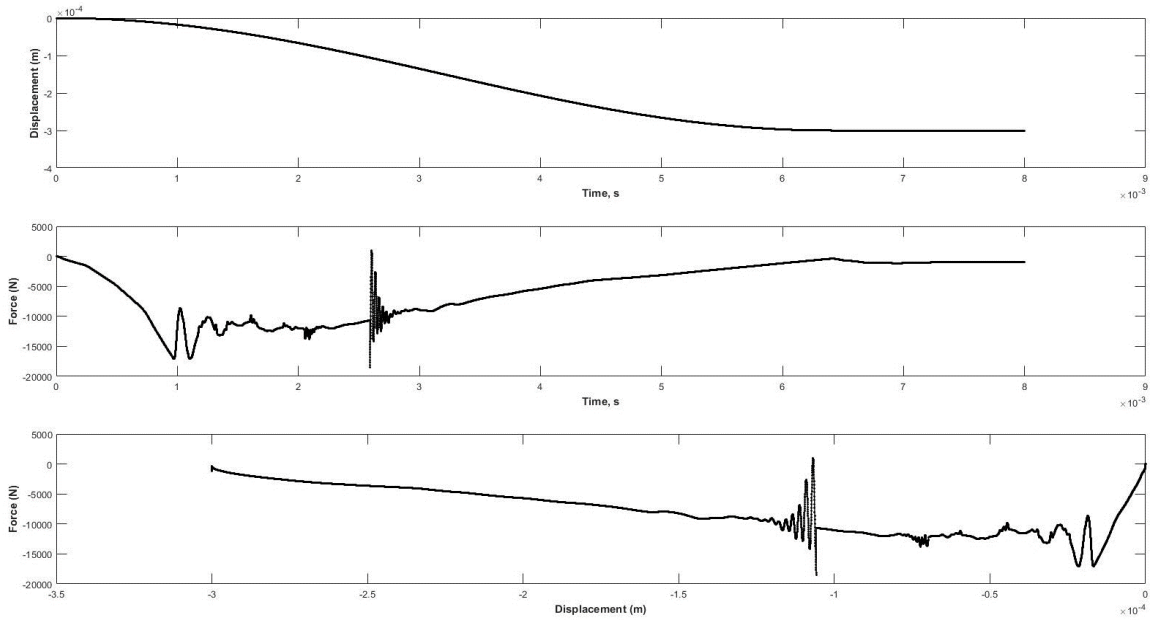

Figure 6.5 (a) Displacement vs. time (b) Force vs. time (c) Force vs. displacement for modulus of rupture test

In the simulation of the modulus of rupture test, the peak load obtained when the lattice is not rotated i.e; at $\theta = 0^0$ is half the peak load obtained for a 30^0 rotated lattice. The damage pattern can be clearly observed in Figure 6.6.

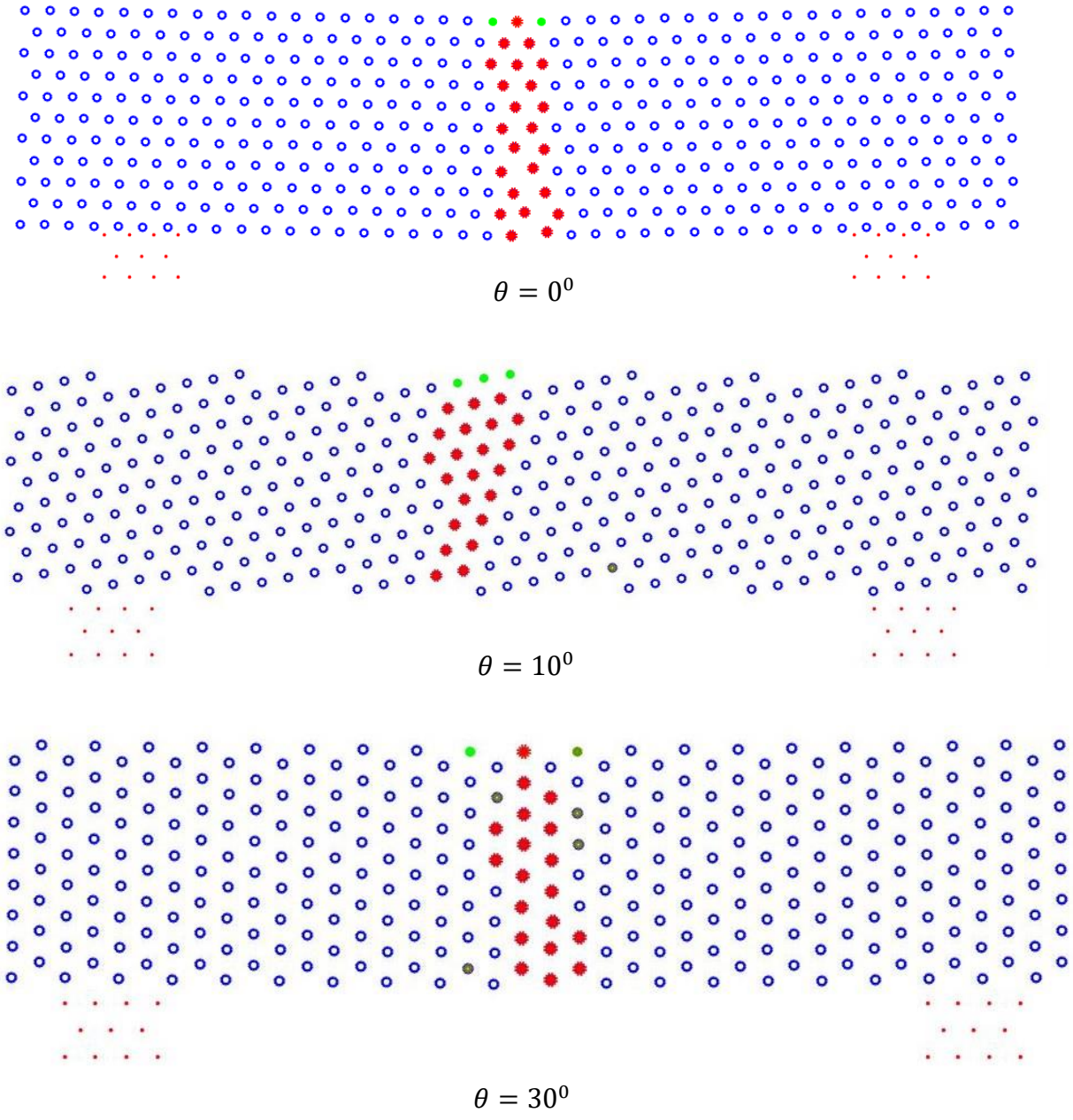

Figure 6.6 Damage patterns as a function of lattice rotation for modulus of rupture test

Chapter 7 Discussion, Conclusions and Future Work

7.1 Summary of Test Results

In this chapter, a summary of the analysis is given. The SPLM results are compared to lab results. Later, the mechanism of failure in split cylinders is analyzed. Some conclusions are made regarding the damage model, the bond configuration and interaction between different lattice bodies in SPLM. The stress distribution in concrete specimens cast in the laboratory is questioned. Later, the testing machine of the SPLM and the concepts of displacement controlled loading and load controlled loading are discussed.

Summarizing all the results obatined from the three test methods, the difference between the peak loads obtained from the laboratory tests and SPLM analysis is given in Table 7.1.

Table 7.1 Peak load obtained from for each test (lab vs. SPLM)

Type of Test	**Lab Results (Wright, 1955)**	**SPLM results**
Brazilian split cylinder test	45.8 kip	126 kip
Direct tension test	3.45 kip	3.72 kip
Modulus of rupture test	2.15 kip	4.07 kip

The peak loads of the laboratory tests were calculated from the tensile strengths listed in (Wright, 1955). This calculation was discussed earlier in section 4.7. For the peak loads obtained from SPLM, classical linear elastic theory would predict the tensile stregth to be as follows

1. Brazilian split cylinder test

$$f_{sp} = \frac{2P_{max}}{\pi LD} = \frac{2 \times 126}{\pi \times 12 \times 6} = 1114\ psi, \tag{6.4}$$

2. Direct tension test

$$F_t = \frac{P}{A} = \frac{3.72}{\pi \times 2^2} = 296\ psi, \tag{6.5}$$

3. Modulus of rupture test

$$\sigma = \frac{M.y}{I} = \frac{\frac{PL}{4}y}{I} = \frac{4.07 \times 12 \times \frac{4}{2}}{4 \times \frac{4^4}{12}} = 1144\ psi. \tag{6.6}$$

Therefore, the comparison of tensile strength obtained from the three tests from laboratory, SPLM analysis as predicted by classical theory is given in Table 7.2.

Table 7.2 Classical theory prediction of tensile strength from each test (lab vs. SPLM)

Type of Test	**Lab Results**	**SPLM results**
Brazilian split cylinder test	405 psi	1114 psi
Direct tension test	275 psi	296 psi
Modulus of rupture test	605 psi	1144 psi

It is observed that the tensile strength obtained from direct tension test is the least compared to the Brazilian split cylinder test and the modulus of rupture test in both SPLM analysis and lab tests. The direct tension test can produce reasonable results if the test is conducted with the appropriate specimen shape. Nevertheless, the direct tension is the most conservative among all the three tests. The classical theory prediction of tensile strength for the Brazilian split cylinder test is higher than the direct tension test but lower than the modulus of rupture test. The lab results also show similar a relationship.

7.2 Split Strength Indicator

To verify if the maximum load, at which the split cylinder fails is dictated by plastification and crushing of concrete under the applied compressive loads or the damage of concrete particles, the SPLM models at different stages of loading are presented in Figure 7.1 indicating concrete crushing and subsequent tensile cracking.

The load corresponding to each stage is indicated in the load versus time step graph shown in Figure 7.1. Diametral tensile cracks are formed but only after significant plastification. The peak load is observed to be 561 kN which corresponds to stage 2. The third stage shown, where the partial damage, yielding and plastification is observed along the vertical diameter represents a load of 527 kN. The final stage where the full damage is observed corresponds to a load of 470 kN.

The peak load occurs well before the tensile crack forms as represented in the Figure 7.1 indicating that the formation of tensile crack in the middle of the cylinder is not the proximate failure mechanism but it is because of concrete plastification or crushing (Gerstle, 2015).

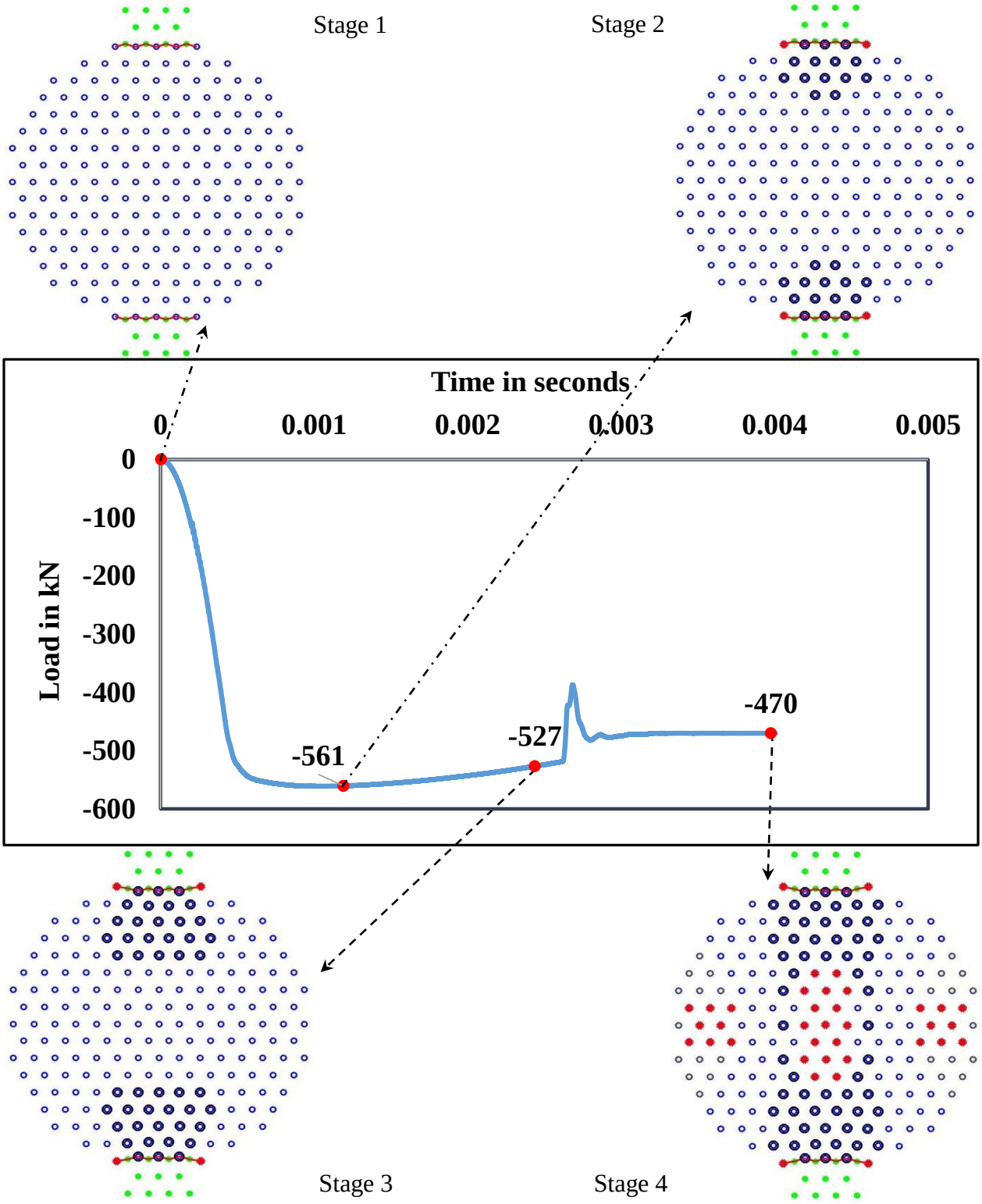

Figure 7.1 Plot of Load vs time for split cylinder

7.3 Stress Distribution in Concrete Specimens

The power of computational analysis allows us to simulate the same concrete cylinder specimen for every analysis. But is that the case when a physical experiment is conducted in the lab? Every specimen is different in its matrix arrangement as shown in Fig. 7.2.

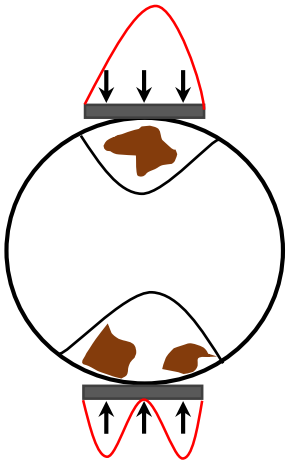

Figure 7.2 Rough sketch of tress distribution showing aggregates

Would the stress distribution be the same at the top and bottom of the specimen shown in Figure 7.2? Not really! Concrete does not hold Hooke's law as the apparent value of Young's modulus decreases with increasing stress (Wright, 1955). The highly stressed parts in a concrete specimen are tend to be relieved by such a stress-strain curve and the additional stress is thrown on to those parts where stress is lower. The load required to break the specimen will therefore tend to increase and thus high values of peak loads may be observed (Wright, 1955). An important aspect here is also the stiffness of loading plate. If the test results depend on the value of stiffness, is it a good test?

7.4 Suggestions for Future Research

Tensile damage in SPLM initiates when the average elastic stretch in a bond is sufficiently high. One possible aspect for future research is to understand if the tensile damage should initiate when the maximum elastic stretch in a bond or a particle reaches a critical value. This would highly improve the crack propagation in SPLM models.

SPLM has immense potential to model reinforced concrete structures. The interaction between different lattice bodies could be perfected to simulate the behavior of any composite structure like reinforced concrete more accurately.

The SPLM models in this thesis are tested by applying a time varying displacement to the steel platens. The testing machine in SPLM is currently displacement controlled and the stiffness is infinity. It would be interesting to know how the model works if the test was load controlled. In laboratory experiments, the splitting test is a load controlled test.

Another interesting aspect in concrete which can be studied is the micro-cracking effect dominant in concrete.

7.5 Conclusions

As computer hardware and software become much more powerful in the upcoming future, the ability to obtain solutions to much larger problems than what were solved in this thesis will be possible within a much lesser time frame with SPLM. The time of simulation, for accuracy within 3%, is 16 x $T_{fundamental}$ and the user can change this value based on the demand of accuracy. The longest analysis for this thesis was for 128 x $T_{fundamental}$ which was around 90000 time steps and this analysis took about 8 minutes on Intel Core 17-4790K CPU @4.0 GHz. The operating system

type is 64-bit and the installed (RAM) has 31.8 GB usable memory. With a much more powerful computer or using parallel computers, this analysis will take even shorter time to finish.

SPLM has the potential and ability to model plasticity, damage, elasticity in practical problems as we have seen. SPLM has the advantages of being simple and extremely user friendly when compared to other contemporary computation modelling techniques. It is well suited to modern digital computers. SPLM has the capacity to predict the behavior of a wide range of materials and to do so, it does not make too many assumptions when compared to classical continuum mechanics. SPLM excels in the simulation of dynamic behavior of structures. Short term dynamic events can be best modelled using SPLM. SPLM powerfully aids in understanding of material behavior.

References

ASTM-C496/C496M , A. (2011). Standard Test Method for Splitting Tensile Strength of Cylindrical Concrete Specimens: ASTM International.

Bazant, Z. P., Kazemi, M. T., Hasegawa, T., & Mazars, J. (1991). Size effect in Brazilian split-cylinder tests: measurements and fracture analysis. *ACI Materials Journal, 88*(3), 325-332.

Boulekbache, B., Hamrat, M., Chemrouk, M., & Amziane, S. (2014). Failure mechanism of fibre reinforced concrete under splitting test using digital image correlation. *Materials and Structures*, 1-14.

Cornelissen, H., & Reinhardt, H. (1984). Uniaxial tensile fatigue failure of concrete under constant-amplitude and programme loading. *Magazine of concrete Research, 36*(129), 216-226.

Gerstle, W., Sau, N., & Silling, S. (2007). Peridynamic modeling of concrete structures. *Nuclear engineering and design, 237*(12), 1250-1258.

Gerstle, W. H. (2015). *Computational Solid Mechanics Without Stress and Strain*.

Griffith, A. A. (1921). The phenomena of rupture and flow in solids. *Philosophical transactions of the royal society of london. Series A, containing papers of a mathematical or physical character*, 163-198.

Hoang, L. C., Andersen, M. E., Hansen, N. T., & Jónsson, T. H. (2014). Strength prediction and failure modes of concrete specimens subjected to the split test. *Materials and Structures, 47*(11), 1953-1968.

Inglis, C. E. (1913). Stresses in a plate due to the presence of cracks and sharp corners. *Spie Milestone series MS, 137*, 3-17.

Irwin, G. R. (1957). Analysis of stresses and strains near the end of a crack traversing a plate. *Spie Milestone series MS, 137*, 167-170.

Kachanov, L. (1958). Time of the rupture process under creep conditions. *Isv. Akad. Nauk. SSR. Otd Tekh. Nauk, 8*, 26-31.

Rojas, R. (1997). Konrad Zuse's legacy: the architecture of the Z1 and Z3. *Annals of the History of Computing, IEEE, 19*(2), 5-16.

Silling, S. A. (2000). Reformulation of elasticity theory for discontinuities and long-range forces. *Journal of the Mechanics and Physics of Solids, 48*(1), 175-209.

Silling, S. A., Epton, M., Weckner, O., Xu, J., & Askari, E. (2007). Peridynamic states and constitutive modeling. *Journal of Elasticity, 88*(2), 151-184.

Truesdell, C. (2012). *The Elements of Continuum Mechanics: Lectures given in August-September 1965 for the Department of Mechanical and Aerospace Engineering Syracuse University Syracuse, New York*: Springer Science & Business Media.

Westergaard, H. (1939). Bearing Pressures and Cra; c];< si. *Journal of applied mechanics*.

Williams, M. (1997). On the stress distribution at the base of a stationary crack.

Wright, P. (1955). Comments on an indirect tensile test on concrete cylinders*. *Magazine of concrete Research, 7*(20), 87-96.